CHARACTERIZATION OF Cu_2S / SnO_2: F P-N JUNCTION FOR SOLAR CELL APPLICATIONS

JARED GISEMBA OMWOYO (B.Ed. Sci.)

I56/CE/24509/12

A THESIS SUBMITTED IN PARTIAL FULFILLMENT OF THE REQUIREMENTS FOR THE AWARD OF A DEGREE OF MASTER OF SCIENCE (PHYSICS) IN THE SCHOOL OF PURE AND APPLIED SCIENCES OF KENYATTA UNIVERSITY.

OCTOBER, 2019

DECLARATION

This thesis is my original work and it has not been presented for award of a degree or any other award in any other University.

Sign..... Date 16/10/2019.

Jared Gisemba Omwoyo

Physics Department

Kenyatta University

This thesis has been submitted for examination with our Approval as University supervisors.

Sign..... Date 17/10/2019

Dr. Mathew K. Munji

Physics Department

Kenyatta University

Sign..... Date 17-10-2019

Dr. Sebastian M. Waita

Physics Department

Nairobi University

DEDICATION

I dedicate this thesis to my mother Maria, my wife Calister, my sons Griffins and Ignatius and my daughter Angela.

ACKNOWLEDGEMENTS

I thank God for giving me good health throughout the research period, indeed this far I have come it has taken His hand. My greatest appreciation goes to my supervisors Dr. Mathew K. Munji of Kenyatta University and Dr. Sebastian M. Waita of Nairobi University for their intellectual support throughout the research period. I also thank all Kenyatta University physics laboratory technicians especially Mr. Abraham Chisaina for their technical assistance and encouragement during my research work. I would like to recognize Mr. Stanley Kariuki a laboratory technician in chemistry department (Kenyatta University) for the assistance he gave me during sample preparation.

Special thanks goes to my colleague students Dennis Okinyi, Michael Kangethe and Evans Ongeri for their encouragement and exchange of ideas during research work. I also express my thanks to Nairobi University physics laboratory technician Mr. Boniface Muthoka for his technical assistance in measuring the optical properties of thin films and measurement of I-V characteristics of the cell. Special thanks also to my wife Calister Bosibori for her constant encouragement throughout my research work, may God bless you all according to His will.

TABLE OF CONTENT

LIST OF TABLES

LIST OF FIGURES

ABBREVIATIONS AND SYMBOLS USED

CBD	Chemical Bath Deposition
Cu_2S	Cupper Sulphide (Copper (I) Sulphide)
DC	Direct Current
E_g	Band Gap
eV	Electron Volt
FF	Fill Factor
FTO	Fluorine- doped Tin (IV) Oxide
IR	Infra-Red
I-V	Current versus Voltage
NIR	Near Infra-Red
PLD	Pulsed Layer Deposition
PV	Photovoltaic
R_s	Sheet resistance
SnO_2: F	Fluorine- doped Tin (IV) Oxide
SPT	Spray Pyrolysis Technique
UV	Ultra Violet
VIS	Visible Spectrum
V_{oc}	Open Circuit Voltage
XRD	X-ray diffraction
ρ_s	Sheet resistivity
η	Conversion Efficiency
α	Absorption Coefficient

ABSTRACT

Due to industrialization and increase in population, there is need for clean, green and renewable source of electrical energy. Traditional sources of electrical energy like fossil fuels are getting depleted, on the other hand silicon based solar cells are expensive hence the need for low cost and reliable alternative source of energy. Photovoltaic is a reliable energy source which is renewable. Photovoltaic is a process of conversion of solar energy to electricity directly using solar cells. For this study Copper (I) Sulphide (Cu_2S) thin films were deposited on glass substrates by Chemical Bath Deposition (CBD) technique. Copper sulphate ($CuSO_4$) was used as a source of copper ions, thiourea ($CS(NH_2)_2$) as a source of sulphide ions and tartaric acid as a complexing agent, ammonia solution was used to regulate the pH. SnO_2: F thin films were deposited using spray pyrolysis technique (SPT) on glass substrates at substrate temperature of 350^0 C using pentahydrated stannous chloride ($SnCl_4 \cdot 5H_2O$) and ammonium fluoride (NH_4F) as precursors. Optical transmittance and reflectance of all film samples prepared in the range of 200 nm-1100 nm were measured using UV-VIS-NIR spectrophotometer. The optical measurements were simulated using SCOUT software to obtain optical constants. Cu_2S deposited at 0.15 M Cu^{2+} exhibited low average transmittance of 20.91 %, high average absorbance of 51.29 % and narrow optical band gap of 2.33 eV hence a good absorber material to be used as p-type layer in solar cells applications. On the other hand, SnO_2: F had high average transmittance of 79.94 % and wide optical band gap of 4.04 eV at 4 % concentration of fluorine. This shows that SnO_2: F is a suitable n-type layer for solar cell applications. Cu_2S had lowest refractive index of 1.44 at 0.15 M Cu^{2+}. The four point probe was used to measure the sheet resistivity of all thin films. SnO_2: F had lowest resistivity of 40.3 Ω cm at 4% concentration of fluorine while Cu_2S had low resistivity of 0.40×10^3 Ω cm at 0.15 M Cu^{2+}. The Cu_2S/SnO_2: F p-n junction was fabricated in phases. First the n-type layer of SnO_2: F was deposited onto the glass substrate by spray pyrolysis method and then the p-type layer of Cu_2S thin films was deposited onto SnO_2: F thin film to form a p-n junction. The solar simulator was used to measure the I-V characteristics of the fabricated cell. The fabricated cell had open circuit voltage (V_{oc}) of 0.4075 V, short circuit current (I_{sc}) of 0.00219 A, fill factor (FF) of 0.61 and efficiency (η) of 0.303 %. Therefore, Cu_2S and SnO_2: F thin films are suitable materials for fabrication of Cu_2S/SnO_2: F p-n junction solar cell.

CHAPTER ONE

INTRODUCTION

1.1 Background to the study

Sun provides free and inexhaustible energy in many forms, among them solar energy. This clean and abundant energy can be solely relied on to offers an alternative option to fossil fuels that are limited and have contributed to water and air pollution. Renewable sources such as solar PV are already playing a vital role in the world's energy supply contributing a sizeable percentage. Solar power is a source of energy with easiness in its installation and maintenance as well as being reliable. A thin film solar cell is made when a substance has been deposited with thin film layers of a photovoltaic material. The solar cell performance is influenced by the film layers' thickness which range up to tens of micrometers (Muller *et al.*, 2004).

Solar electricity more so photovoltaic conversion is forming a major component in energy industry currently since a stand-alone system which is fuel free is highly reliable and abundance of sunlight especially in tropics. A solar cell function by photogeneretion of charge carries in the light absorbing material and then charge carrier separation to a contact that conduct and then offer electricity transmission.

The photovoltaic cells are composed of two layers which include an n-type and p-type layers (Ezema *et al.,* 2010). When the photons of the sun reach the solar cell they can be transmitted, absorbed or reflected depending on the window material, the dopants and the wavelength of light. Only absorbed photons generate electricity by creating and separating charges in the cell. XRD studies show that thin films of oxides of tin that have been doped with fluorine and preparation done using glass substrate by the

technique of advanced spray pyrolysis technique are all polycrystalline and have a tetragonal crystal structure and they are semiconductors with n-type electrical conductivity (Yousaf *et al*., 2008).

1.2 Statement of the research problem

Non-renewable sources of energy forms a large part of energy that is being used globally, there is a concern over the exploitation of these sources. In addition the silicon based solar cells are expensive. Hence there is need for research to be carried out on a low cost solar energy source in terms of raw material and method of production.

1.3 Objectives

1.3.1 General objective

To fabricate and investigate the properties of Cu_2S/SnO_2: F p-n junction for solar cell applications.

1.3.2 Specific objectives

i. To prepare Cu_2S and SnO_2: F at varying Cu^{2+} and F^- concentrations using CBD and SPT methods respectively.
ii. To measure transmittance and reflectance of all films samples deposited using a UV-VIS-NIR spectrophotometer.
iii. To determine the optical band gap of all films deposited using SCOUT 98 software.
iv. To calculate resistivity of Cu_2S and SnO_2: F films using the four point probe technique.

v. To fabricate Cu_2S/SnO_2: F p-n junction and calculate its cell parameters such as open circuit voltage (V_{oc}), short circuit current (I_{sc}), fill factor (FF) and efficiency (η).

1.4 Rationale

The growing demand for materials with desirable properties such as direct band gap are required in the fabrication process of a solar cell to convert solar energy into electrical energy directly (Elangovan and Ramamurthi, 2003). The high cost of silicon based solar cells and over-exploitation of non-renewable energy sources has necessitated the search for newer photovoltaic devices that are prepared by chemical processes that are of low cost in terms of installation.

Large arrays of photovoltaic cells are used to power spacecraft, to provide electricity in the rural areas which are beyond transmission lines (Kassim *et al., 2008*). Cu_2S/SnO_2: F p-n junction thin film can be used as an alternative photovoltaic cell since Cu_2S is a low cost semiconductor compared to silicon based and other semiconductors being used presently for terrestrial applications (Kumar *et al.,* 2014). This is because Cu_2S are crucial materials for use in p-type semiconductors and optoelectronics. This finds use in photothermal conversion applications and photovoltaic applications (Mehra *et al.,* 2014).

Tin (IV) oxide (SnO_2) has many advantages as a window layer in photovoltaic cells due to its better electron acceptance which gives it a conduction band edge that is more positive. In addition, it has better long-term stability under Ultra-violet illumination (Tatar *et al.,* 2013). Thus Cu_2S/SnO_2: F p-n junction will be investigated for its suitability as a solar cell material.

CHAPTER TWO

LITERATURE REVIEW

2.1 Introduction

Sun gives solar energy in form of radiant heat and light that is harvested using techniques that are always advancing such as photovoltaic, artificial photosynthesis, solar thermal and solar heating. It is an essential source of energy that is renewable which has technologies that are classified broadly into either active solar or passive solar. It has made an appealing electricity source because of it availability in huge amounts.

2.2 Related researches done

2.2.1 Copper (I) Sulfide

Previous research work done on Copper (I) Sulfide thin films has revealed some properties of Copper (I) Sulfide (Cu_2S). The aspects considered included the fabrication of Cu_2S thin films using electrodeposition and Chemical Bath Deposition (CBD) methods. Copper (I) Sulfide deposited by electrodeposition method on the glass substrate has a direct band gap of 2.26 eV material. High deposition temperature leads to the formation of crystalline films. The optimum deposition temperature is 75 ^{o}C (Thanikaikarasan *et al.*, 2010).

The growth rate of Copper Sulfide prepared by Chemical Bath Method shows that the growth rate of the film depends on temperature and the concentration of $CuSO_4$ (Copper Sulphate). It exhibit transmittance which is high from 670 nm and the band gap varies from 1.6 eV to 2.7eV depending on the thickness and the sulfur content (Abbas and Ghdeeb, 2015).

Optical properties of Cu_2S film deposited by CBD were found to have the band gap ranging between 2.64 eV to 2.92 eV. (Kumar *et al*., 2014). The bath composition aided in increasing the band gap as well as annealing of Copper Sulfide thin film.

2.2.2 Fluorine Doped Tin (IV) Oxide

The concentration of fluorine in SnO_2: F increases the band gap from 3.49 to 4.49 eV and resistance increases from 5.0 x 10^9 to 2.11 x 10^{11} Ω-cm (Hassanien *et al.*, 2016).

Several methods have been applied in depositing tin oxide films that have been doped with fluorine, including electro – deposition, spray pyrolysis, and chemical bath deposition (Elangovan and Ramamurthi, 2003). The current-voltage curves shows a decrease in conductivity as the deposition temperature increases and the relationship is almost linear.

Ebrahimias *et al*. (2011) also researched on deposition of nanocrystalline SnO_x (x=1-2) thin films using CBD technique. The SnO_x thin films obtained had a structure that is polycrystalline in nature and has an average grain size of 36 nm as analyzed by x-ray diffraction. The films had direct and indirect transitions in the visible spectrum with band gap values of about 3.8 eV and 3.6 eV respectively.

2.2.3 Copper Based Solar Cells

Ezema *et al.* (2010) reported on the fabrication of Cu_2S/CdS thin film solar cell on ITO-coated plastic substrate. The studies reveals the V_{oc} value higher than 0.54 V which is the conventional value. The cell parameters studied include I_{sc}=5.625 mA/cm^2, fill factor (ff) = 0.494 and conversion efficiency (η) = 1.604 %. Fukuda and

Ichimura (2013) deposited thin films of copper sulphide onto various substrates (glass and polymers) is made possible because of these characteristics giving the application of materials for either radiation control coatings, electric or electronic devices.

The SnO_2/Cu_2O p-n junction is being investigated by researchers in identifying the preparation methods for thin films with good quality due to the wide application of semiconducting materials in electric and electronic devices (Sandeep, 2008).

Many researchers have done a lot of research on fabrication of p-n junction solar cells using Cu_2S as an absorber layer with other materials such as CdS as window materials. In this work, Copper (I) Sulfide (Cu_2S) was used as an absorber layer with highly transparent and conductive SnO_2: F as a window layer in the fabrication of Cu_2S / SnO_2: F and the cell parameters were determined.

CHAPTER THREE

THEORETICAL CONSIDERATIONS

3.1 Introduction

A solar cell works by photovoltaic effect. Converting solar energy into electricity directly. A solar cell work by photo-generation. It is always kept thin for light to pass through the n-type material to the p-type, light travels in packets of energy called photons.

3.2 Photovoltaic Effect

Both chemical and electrical processes are involved in creating current and voltage in a semiconductor when exposed to light. In a solar cell electron-hole pair is created when light is absorbed. The light that is incident to a p-n junction solar cell is transmitted through the n-type material to the p-type semiconductor which absorbs it leading to generation of electron-hole pair. Some of the charge carries with generated minority are swept by electric field to across the junction in the depletion region. The electrons are collected at n-type region while holes are collected at p-type region. Photocurrent is kept connected through the collection of the charges across the cell.

A semiconductor does not absorb all the light that is incident to its surface, part of the light is transmitted through the material and also a portion of the light is reflected by the surface of the semiconductor.

Electron-hole pair is only produced by absorbed light. The absorption coefficient is a parameter that measures the ability of the material to absorb light (Khallaf *et al., 2009*). Electrons in the valence band absorb photons that have energy that is greater

than the band gap which makes them to be excited to states that are higher. An electron-hole pair is created when the electrons that have been excited cross the band gap and move to the n-side. The electron-hole pair is separated by internal electric junction field, the electrons move towards the n-side while holes to the p-side (Satosh *et al., 2008)*.

3.3 Deposition techniques of thin films

Deposition techniques are broadly categorized into physical or chemical methods. There are different chemical and physical methods used to prepare thin films. The main physical methods for preparation of thin films are physical vapor deposition (PVD) and sputtering (Ebrahimias *et al.*, 2011). The chemical methods are spray ion layer gas reaction (spray-ILGAR), deposition (ALD), (CBD), (SILLAR) and chemical spray pyrolysis (CSP). Chemical composition, crystalline and optical properties of the films depends on deposition method used (Sumanta *et al.,* 2012).

3.3.1 Chemical Bath Deposition (CBD) method

This method involves controlling precipitation of compounds from a solution on a substrate. It has more merits than the more advanced methods like MBE, CVD, and spray pyrolysis. The preparation of the first CBD thin films took place in 1884 with the methods being limited for a long time to PbS and PbSe. However, several materials of chalcopyrite and chalcogenide have been deposited after CdS was deposited. Apart from glass, other materials have been used as substrate are ebonite, iron, steel, porcelain and brass (Kumar *et al*., 2014).

The advantage of using CBD method to deposit thin films are: the method is simple in terms of its set up, it is cheap, it enables deposition over a large area, can be carried out at room temperature since the chemical do not require high vacuum, the film deposited by CBD are uniform and can be reproduced and can be used for photovoltaic applications. Chemical bath method is a low cost deposition technique which can be used in industries for large scale production of thin film and also the crystallite size of films deposited by CBD is very small (Fayroz *et al*., 2016).

In chemical bath deposition the measures of deposition such as pH of the solution, complexing agents used, temperature, and precursor concentration can be varied to have a control of the thickness of the film as well as the chemical deposition. The most attractive merit of chemical bath deposition method is its ability cover a large area in coating in a process that is cheap and reproducible. Chemical bath deposition is the simplest method for deposition of films which uses aqueous solution; deposition on a large area can be done using this method without necessarily using instruments that are sophisticated. Proper optimization of the conditions for bath deposition can be used to control and vary the properties of the deposited material.

Using suitable substrates to form a solution of a compound with controlled precipitation is the basis of the CBD method. Immersion into an acidic or alkaline solution is done for the substrate which contains a chalcogenide source, a complexing agent, the added base or acid and a metal ion. Various agents for complexing have been used in thin film deposition which include; sodium hydroxide (NaOH) and triethylamine (TEA).

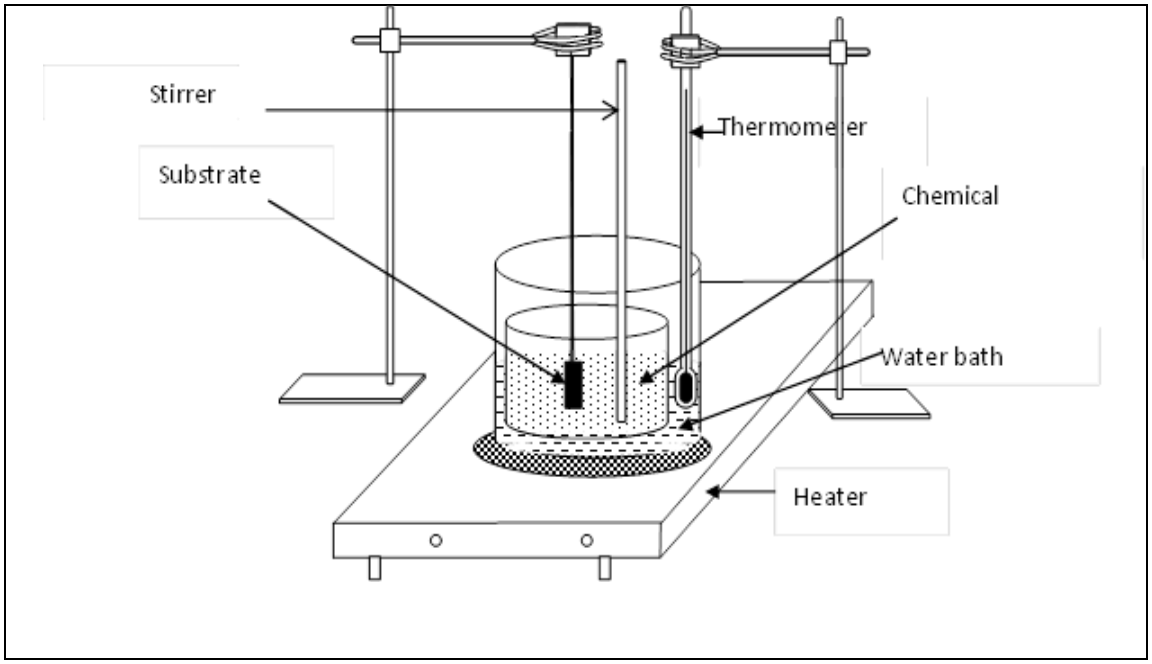

Fig.3.1: Chemical Bath Deposition set up (Sasikala *et al.,* 2000)

Three parts are the basic composition for a chemical bath solution which include; a source of chalcogenide x^{-m} (where x = oxygen, sulphur or selenium), a salt of metal M^{+n} and a complexing agent in aqueous solutions. Selection of the metal salts is based on their solubility from a moderate to a highly soluble salt and the end product that is desired. The rate of generation of x^{-m} and the end product that is desired are used to select the chalcogenide source. The rate of free metal ions generation is used to select the complexing agent which prevents the rapid bulk precipitation of the compound that is desired. It does this by preventing precipitation of metal hydroxides and through the provision of ligands (Ehtenshamul *et al., 2013*).

Formation of films by CBD is determined by concentration of complexing agent, type of the substrate, the precursor solution, and deposition time, temperature of the bath and pH of the solution. The rate of reaction is influenced by an important factor as bath temperature. Greater interaction between ions occurs with increase in the

kinetic energy of the molecule. The thickness of the film then increases or decreases depending on the solution saturation (Makori *et al.,* 2017).

The precursors used affects the growth and the composition of the film that is formed. For example, thickness increases and the rate of deposition decreases when the metal Selenide film is deposited by metal sulphate. Here, the concentration of Selenide ions is reduced from metal sulphate ions obtained from SO_4^{2-} ions. The concentration of ionic precursors increases with the increase in the rate of deposition and terminal thickness.

However, the thickness of the film decreases at higher concentration as the precipitations become very fast. The complexing agent influences the final product to a large extent. The increase in the concentration of the complexing ion also increases the metal ion concentration in a reaction. Consequently, a large terminal film thickness is formed due to a reduction in the precipitation and the rate of reaction. An increase in the pH of the reaction bath increases the stability of the metal complex which reduces the number of free metal ions that are available hence a reduced rate of reaction that increases the thickness of the film.

3.3.2 Chemical Spray Pyrolysis (CSP) method

CSP is a non-vacuum method for deposition of large area films with relatively low production cost and technological abilities for mass production (Muller *et al.,* 2004). Chamberlin and Skarman used this method in 1966 to deposit CdS films. Several depositions have been done since then using the CSP method, such as different metal sulfides e.g. CdS, ZnS, SnS, Cu_xS, $CuInS_2$ and metal oxides, such as CdO, ZnO, TiO_2 SnO_2 and MgO with device applications like sensors, solid oxide fuel cells,

solar cells, and other devices (Dzhafarov *et al., 2006*). Figure 3.2 shows spray pyrolysis deposition system.

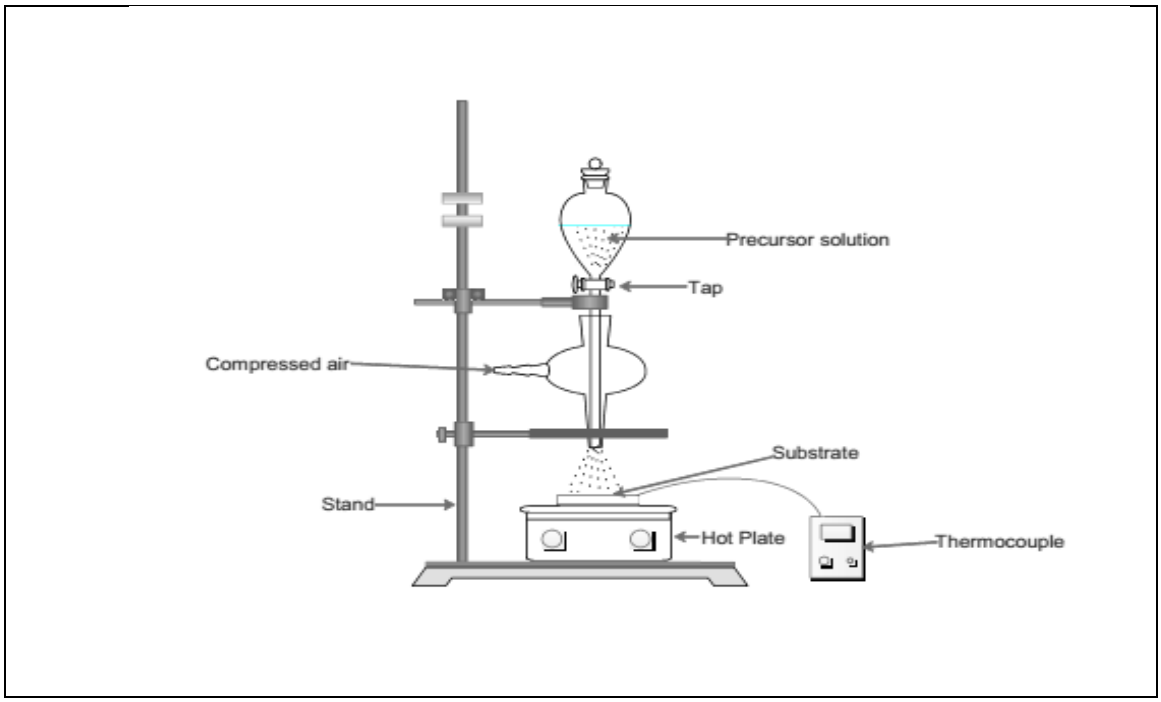

Fig.3.2: Spray pyrolysis deposition system (Saliha, 2006).

Using the CSP process alcoholic or aqueous solution of precursor chemicals is broken into fine droplets to the substrate that has been heated to form the thin film. The CSP equipment set-up consists of an atomizer, which generates very fine droplets of a precursor solution, a substrate heater, a temperature controller and a solution container. CSP techniques can be divided into pneumatic, ultrasonic and electrostatic spray modes depending on the method of generating atomization of the precursor solution. In the pneumatic CSP mode the droplets of the precursor solution, generated by the atomizer are sprayed with the help of the carrier gas onto the preheated substrate.

In the ultrasonic CSP mode the solution droplets generated with the help of an ultrasonic actuator with smaller size and are broken with much lower velocity compared to that by the pneumatic CSP. In the electrostatic CSP mode the fine, uniform, self-dispersive droplets are sprayed with the help of high electrical field applied between spray nozzle and substrate. The disadvantages of the CSP are related to the difficulties with precise surface temperature determination during the film deposition process, the three-dimensional growth mechanism of film and limited number of precursors for different film, because the precursor salts must be soluble in the used solvent. Despite these disadvantages, different metal oxide films have been successfully made by CSP. Metal sulfide films with device quality can also be deposited by CSP, however due to an open system the unwanted oxidation can take place during the film growth (Sumanta *et al.*, 2012).

3.3.3 Physical vapor deposition.

This is a common technique of deposition among the processes that are applied in thin films, thermal evaporation is among the cheapest and oldest techniques which is simple and used with vacuum techniques. Materials are heated till they form vapor in thermal evaporation. The atoms and molecules that are formed out of the evaporant form a vapor cloud that easily condenses on every surface that is exposed to it to form a film. Atomic kinetic energy in solid increases with an increase in temperature that forms the vapor state if heating is continued.

Putting evaporant in a form of powder is the commonest way to form vapor in the batch type to form a refractory metal boat. The evaporant gets high resistance from the boat. An electron beam melter is used to increase the rate of heating of the

evaporant as well as melting it at temperatures that are very high. An impingement of a beam of an electron is used to heat and melt the evaporant after it is placed in a refractory metal-crucible or ceramic.

To make a curve that impinges on the evaporant placed in the crucible, a bent is made on the magnets to correspond to the curve. Water cooling is done to the crucible and EB gun. Deposition of the thermal evaporation film will then occur in any of the substrates that may include metal, plastic, ceramic, and even on leather. A net attraction can occur on the substrate surface in case the deposition is applied to a surface that has been automatically cleaned between atoms present in the deposited film. This kind of bonding is referred to as Van der Waal. The film does not penetrate into the substrate. If the substrate reacts with the evaporant, chemical bonds can be obtained easily.

The difference in the vapor pressures of the components of alloys makes their evaporation to be difficult hence they are not evaporated congruently. Additionally, there exists a difference in the composition of the evaporant and the condensate. Flash evaporations or two source techniques are preferable to depositions with a single source for these compounds. The problems that are associated with evaporation of non-congruent evaporant from a single source can be solved by using two or more sources. However, this needs to be done under careful control of temperatures.

Most of the materials for thin films use a standard and reproducible method of thermal evaporation. The substrates need to be placed at a tangential position to the holder to have good uniformity of thickness. The boats of molybdenum are used to hold the

materials that will be deposited. To avoid any increasing in internal pressure, a re-evacuation is necessary between any two deposition steps for the working chamber. It is essential to clean all the parts with Acetone or Alcohol before the deposition the vacuum evaporator.

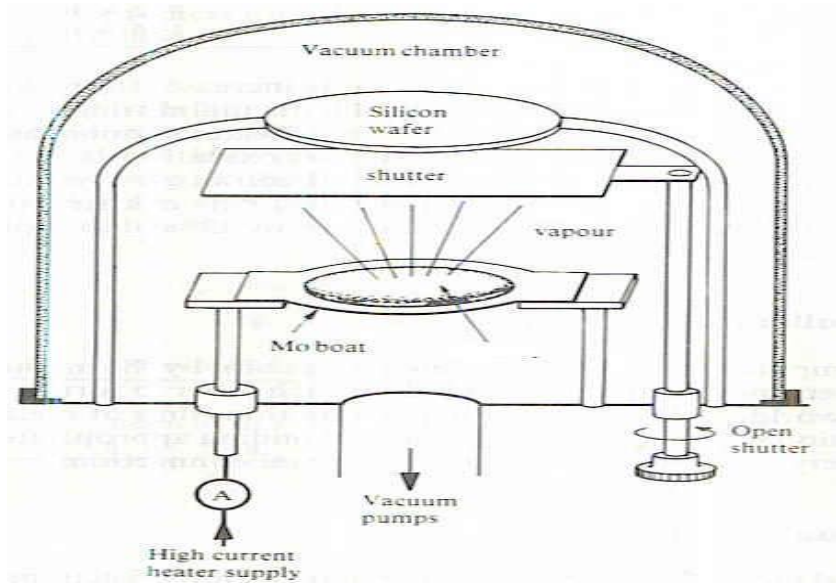

Fig.3.3: A diagram of PVD technique set up (Ashour, 2006).

3.3.4 Sputtering

Sputtering is a technique of thin film deposition where atoms are dislodged from solid target (source) surface to the substrate through impact of gaseous ion mostly argon. In this method dislodging of atoms from the target surface is done by using bombardment of the energy particle to eject atoms that will then be condensed as thin film on a substrate.

Lower temperatures are used to release atoms from the source in sputtering than in evaporation technique where a target is placed in a vacuum chamber with introduction

of inert gas at low pressures. RF power source then strikes the gas plasma to ionize the gas. The deposition time is adjusted and the operating parameters fixed to control the thickness of the thin film.

3.4 Energy bands in solids

The energy gap in a semiconductor provides it with the optical absorption. Photons are absorbed in the process as electrons get excited as they move to conduction bands that are not occupied from valence bands that are not free (Omari, 1975). However, if the energy is not more than the gap energy, the process will not occur, hence photon absorption not be effected. This shows that the material is transparent to electromagnetic radiation but does not reflect it for which ($h\omega<E_{gap}$) (Guoshi *et al.,* 2004*)*.

Additionally, other processes can be obtained for ($h\omega>E_{gap}$*)*, such as inter band absorption. The density state increases sharply at the band edges of semiconductors that contain high quality crystals with low temperatures causing a sharp increase in the time of absorption when photon energy is being obtained by the gap energy. Observation of the optical edge of absorption is used to determine the energy in semiconductors (Gutierrez *et al., 2002*).

This condition is achieved readily when the lowest of the CB and the highest of the VB occur at the same *k*-value (often $k = 0$ as in the diagram below). Figure 3.4 (a) shows a direct band gap structure. The gap is called indirect band gap when the valence band highest and conduction band highest do not occur at the same *k*-value Fig. 3.4 (b). For momentum and energy to be converted at the band gap, a phonon is

usually necessary to participate as another particle for indirect transition absorption. In these processes, there is the participation of a phonon which will make transition probability be lower.

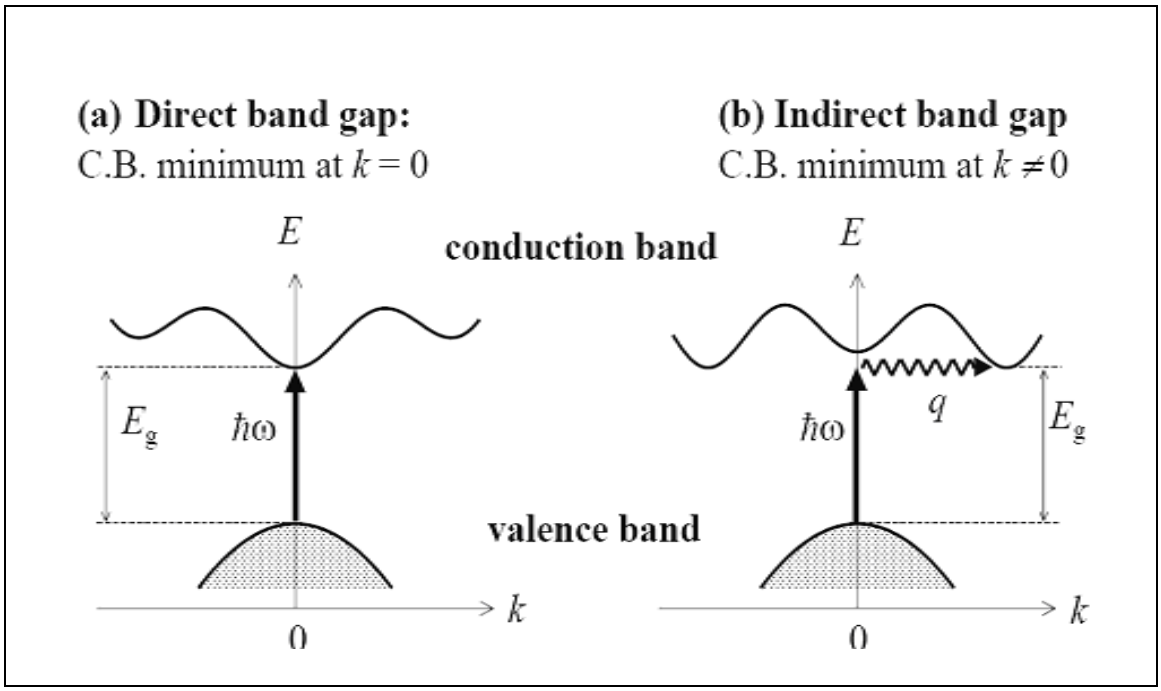

Fig. 3.4: Direct and indirect band gap (Philipps, 2015).

3.5 Optical characterization

The optical characteristics of a semiconductor like energy gap (E_g), refractive index and absorption coefficient are very important parameters in understanding the optoelectronic properties of a material. Transmittance and reflectance data of the thin films are measured using a spectrophotometer machine.

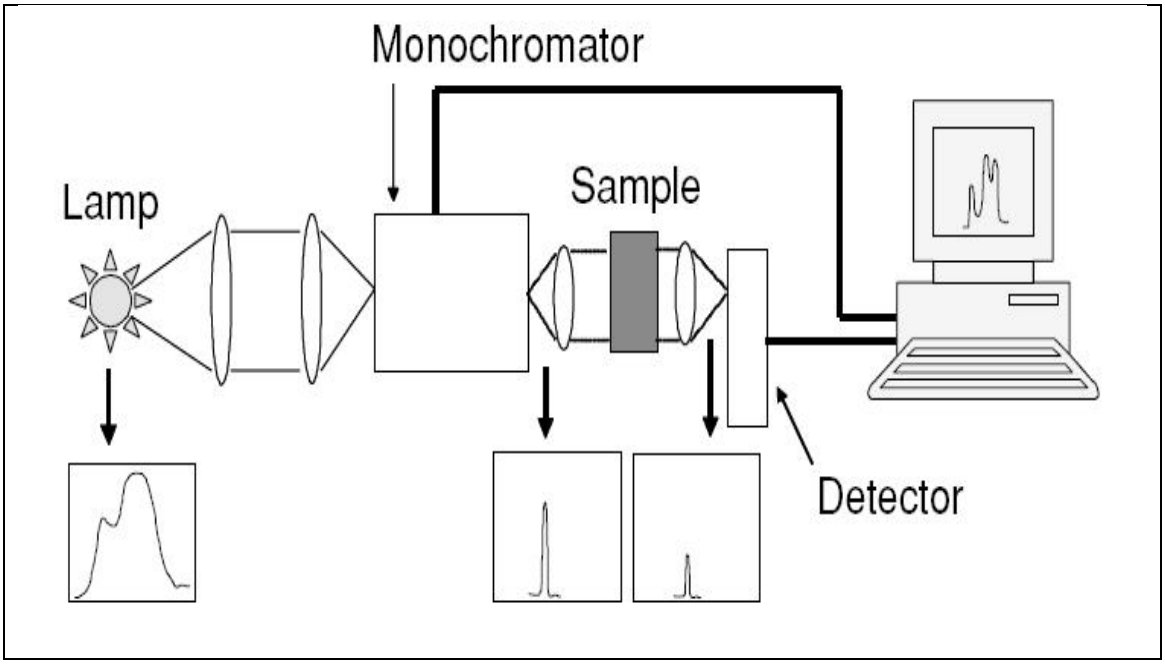

Fig.3.5: A schematic diagram a spectrophotometer machine (Hani *et al.*, 2008).

The spectrophotometer has two sources of radiation; a UV range from the deuterium lamp and visible (VIS) and near infrared (NIR) range from a halogen lamp. During the assessment of wavelength range, the source of radiation changes automatically to make measurements. Relative transmissions are observed for photons with selected beam intensity I_o (photons/cm^2-s) and wavelengths with focus on the thickness of the thin film. Absorption occurs for photons that have energies greater than the band gap (E_g) while transmission occurs for those that have less energy. Transmittance of a material is calculated using Beer Lambert's law (Morumbwa, 2013).

$$I_t = I_o e^{-\alpha l} \tag{3.1}$$

Thus Transmittance is calculated from equation 3.2;

$$\text{Transmittance}(T) = \frac{I_t}{I_o} \tag{3.2}$$

Reflectance (R) of the film is given by;

$$\text{Reflectance(R)} = \frac{I_R}{I_o} \tag{3.3}$$

where I_o and I_R are incident and reflected beam intensities, adopted from Morumbwa (2013).When light traverses through a material, some energy is absorbed. Absorption coefficient, α is determined using equation 3.4;

$$\alpha = \frac{1}{l} \ln\left[\frac{I_o}{I_t}\right] \quad (cm^{-1}) \tag{3.4}$$

where α is the absorption coefficient, I_o and I_t incident and transmitted intensities and ι is the thickness of the film.

Optical constants such as the absorption coefficient and optical band gap and refractive index are analyzed by SCOUT 98 (Dzhafarov *et al*., 2006) given by;

$$n = 4.08 - 0.62E_g \tag{3.5}$$

The direct optical band gap, E_g of the thin films is determined from the standard expression given below (Ogwu *et al*., 2007);

$$\alpha (h\nu) = A (h\nu - E_g)^{1/2} \tag{3.6}$$

where; α is the absorption coefficient, A is a constant, $h\nu$ is photon energy. The optical band gap will be obtained by extrapolating the linear region of the graph of $(\alpha h\nu)^2$ verses $h\nu$ (photon energy).

Relative transmissions are observed for photons with selected beam intensity I_o (photons/cm^2-s) and wavelength. Absorption occurs with photons having energies greater than band energy while transmission for those having energy less than band gap (E_g). This can give accurate measurement of band gap (E_g).

3.6 Electrical characterization

3.6.1 Four point probe method

This is a method that is used to measure resistance of thin layers by allowing the current to pass through the outer two points and measuring the voltage in the two inner points as shown in fig. 3.6. In figure 3.6 the sheet resistance is measured by sending direct current through the two outer probes and the induced voltage is measured using the two inner probes. The thickness of the film is obtained from SCOUT software. Measurements in the four point probe is made by making contact in the four terminals of the probe.

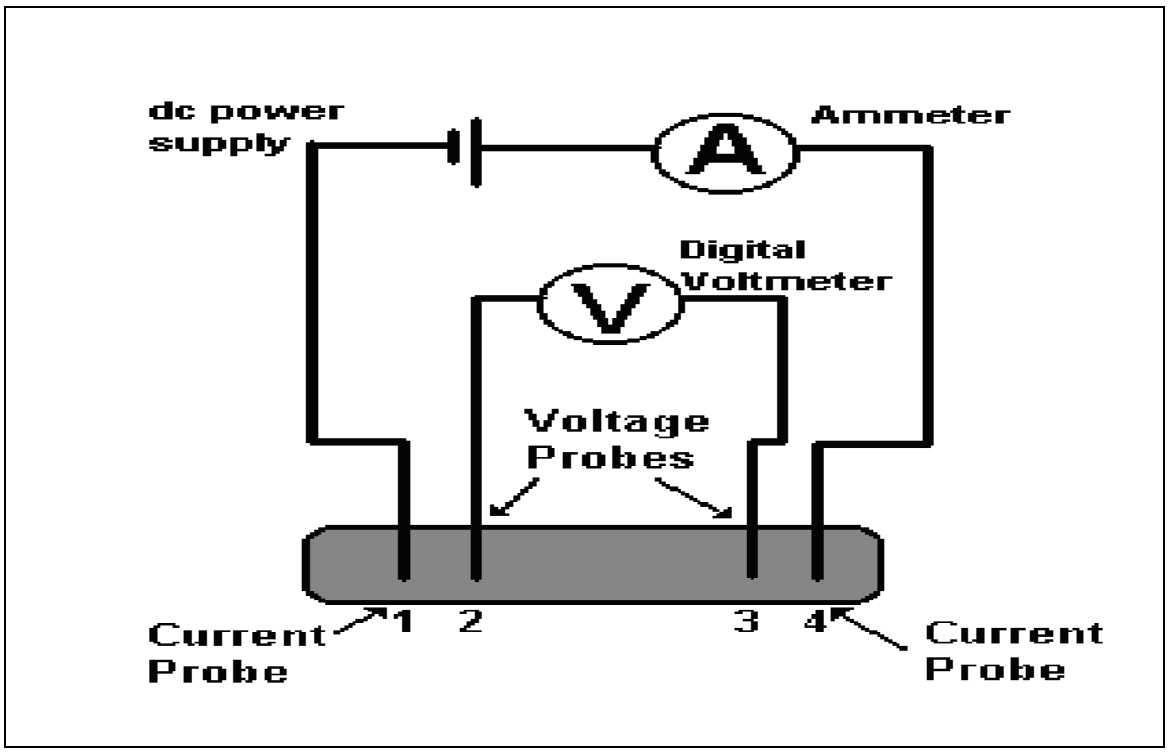

Fig.3.6: A diagram of four point probe measurement (Brown and Jakeman, 1996).

For a thin film sample of thickness t very small compared to its cross sectional area (A) where $A=2\pi xt$, we have a case of current rings so that;

$$R_s = \int_{x1}^{x2} \rho \frac{dx}{2\pi xt} = R_S = \int_s^{2s} \frac{\rho}{2\pi t} \frac{dx}{x} = \frac{\rho}{2\pi t} \ln x \Big|_S^{2S} = \frac{\rho}{2\pi t} \ln 2$$

(3.7) where; t is the film thickness, R_s is the Sheet resistance x length of the sample and π is pie.

The sheet resistivity for thin films will be calculated using the equation 3.8

$$\rho = \frac{2\pi t R_s}{\ln 2} \quad (3.8)$$

Due to superposition of current at outer two tips, sheet resistance is given as;

$$R_s = \frac{V}{2I} \quad (3.9)$$

The film thickness is obtained from SCOUT software. Sheet resistivity can be calculated using;

$$\rho_s = 4.532t \frac{V}{I} \quad (3.10)$$

where; t thickness of film , V is the voltage and I is the current.

3.7 Characterization of the p-n junction solar cell.

Current-voltage characteristics of the cell are shown in fig.3.7. The highest voltage developed by the cell is V_{oc} and highest current of the cell is I_{sc}. The maximum power of the cell (P_m) is given by $P_m = V_{oc}\, x\, I_{sc}$ when the cell delivers maximum current and voltage. However, the actual power is given by $P_m = V_m\, x\, I_m$. Solar cell characterization techniques enables the users to assess the performance of the device, the conditions that affect its performance and give the material characteristics (Jaehyeong *et al., 2009*).

Conversion efficiency is the most essential measure in the solar cell characteristics which depends on spectral content of illumination source. Accurate device

performance can be arrived at with current- voltage curve measurements shown by Fig. 3.7, where V_{oc} is open circuit voltage, I_{sc}- is short circuit current. V_{mp}- is voltage at maximum power point, I_{mp}- is current at maximum point MPP- is the maximum power point.

Solar cell I-V characteristics curves provide the needed information to configure the cell so that it can operate within its maximum power point.

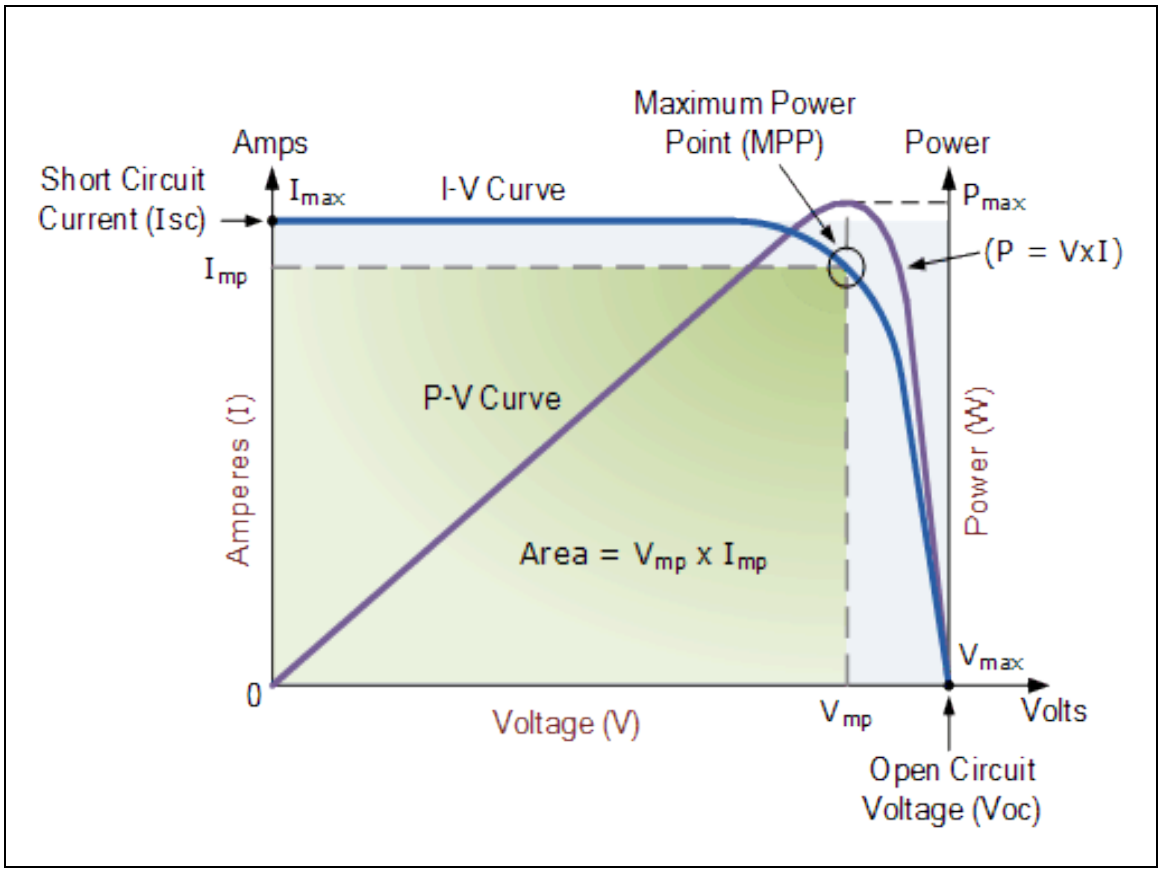

Fig.3.7: Current-voltage Curve of a solar cell (Shah *et al.*, 1999).

Maximum power point is measured as the solar cell produces its maximum amount of power when exposed to solar radiation equivalent to 1000 watts per square meter, 1000 W/m^2 or $1kW/m^2$. Reverse bias increases the junction potential.

This generates small current I_o (dark saturation current). I-V characteristics are given by Shockley equation as shown below (Markvart, 1998);

$$I = I_o\left(\exp\left[\frac{qV}{kT}\right] - 1\right) \quad (3.11)$$

where I is current, I_o is dark saturation current, V is voltage, K is Boltzmann's constant (8.62 x 10^{-3}eV/K), q is electron charge and T is absolute temperature.

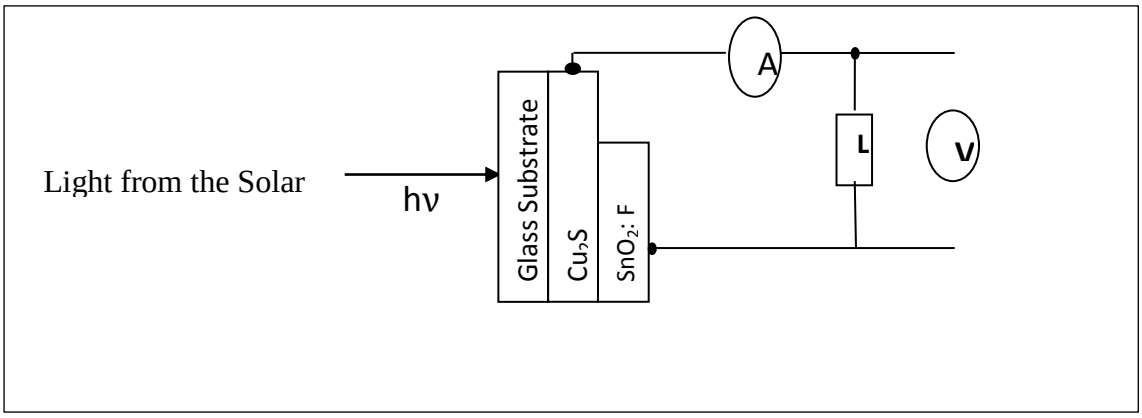

Fig.3.8: Schematic diagram for measurement of diode characteristics (Kassim *et al*., 2010).

The solar cell efficiency is characterized using several measures, including the maximum power point (P_{max}), the short circuit current (I_{sc}), and the open circuit voltage (V_{oc}). The maximum power point (P_{max}) is the product of the maximum cell current (I_{max}) and the voltage (V_{max}) where the power output of the cell is greatest. This point is located at the "knee" of the curve as shown in figure 3.7.

The largest current is obtained when the diode is under the short circuit condition. Short circuit current (I_{sc}) is given by;

$$I_{sc} = I(V = 0) = I_L \quad (3.12)$$

where I_L is the light generated current.

Open circuit voltage, V_{oc} is obtained by setting I=0, is given by (Markvart, 1998);

$$V_{oc} = \frac{AkT}{q} \ln\left[\frac{I_L}{I_o} + 1\right] \quad (3.13)$$

The power output is defined as;

$$P_{out} = V_{out} \times I_{out} \quad (3.14)$$

P_{max} provided by the cell is achieved at a point on the characteristics, where I x V is maximum. From P_{max}, fill factor (FF) which gives the quality of the cell can be calculated as given by (Tiwari, 2009);

$$FF = \frac{V_{max} I_{max}}{V_{oc} I_{sc}} \quad (3.15)$$

The efficiency (η) of the cell can be calculated using equation (3.16).

$$\eta = \frac{V_{max} I_{max}}{P_{in}} = \frac{V_{oc} I_{sc} FF}{P_{in}} \quad (3.16)$$

where (P_{in}) is total radiation incident on solar cell.

CHAPTER FOUR

EXPERIMENTAL PROCEDURES

4.1 Introduction

In this chapter chemical bath and spray pyrolysis deposition methods and experimental procedures involved in both methods and how to clean the glass substrate to be used for deposition and characterization of Cu_2S and SnO_2: F films is discussed extensively. At the end of this chapter, fabrication and characterization of Cu_2S / SnO_2: F p-n junction solar is discussed.

4.2 Cleaning of the substrate

The microscope glass slides which were used were washed with tap water and then washed with deionized water several times, after which they were washed with detergent solution. They were then washed with deionized water and then air dried (Kumar *et al.*, 2014).

4.3 Thin film deposition

4.3.1 Deposition of Cu_2S films

Cu_2S was deposited using chemical bath deposition method. Copper sulphate was used as a source of Cu^{2+} and thiourea [CS $(NH_2)_2$] which was the origin S^{2-}. The molarities of copper sulphate was varied from 0.05 M to 0.20 M to get the optimum concentration. The complexing agent used was tartaric acid. A uniform reaction bath was formed by dissolving the compounds in distilled water. The pH was regulated by ammonia.

4.3.2 Experimental set-up for CBD

Figure 3.1 (page 10) is a set up for chemical bath deposition (CBD). The substrate was vertically dipped into the solution. The heater raises the temperature of the precursor solution and increases the rate of reaction. The thermometer was used to measure the temperature.

4.3.3 Deposition of SnO_2: F (n-type)

Spray pyrolysis technique was used to prepare SnO_2: F thin films. The reagent which were used in preparing fluorine doped tin oxide (SnO_2: F) thin film were stannous chloride ($SnCl_2.5H_2O$) as a source of tin ions (Sn^{2+}) and ammonium fluoride (NH_4F) as a source of fluoride ions (F^-). Hydrochloric acid (HCl) was used to dissolve stannous chloride and Propan-2-ol ($CH_3CHOHCH_3$) was also used as a solvent.

4.3.4 Experimental set-up for Spray pyrolysis.

Figure 3.2 (page 12) is a set up consisting of a retort stand to hold the spray pyrolysis equipment which carries the precursor solution and has a hole to let in air from the air compressor. The hot plate was used a heating source.

4.4 Procedure

4.4.1 Deposition of Copper (I) Sulphide films

The composition of the bath solution used in deposition of Cu_2S is given in table 4.1.

Table 4.1: Constituents of the solution for depositing Cu_2S

Copper sulphate ($CuSO_4$)		0.1M $C_4H_6O_6$	0.1M $CS(NH_2)_2$	Time (min)
Concentration	Volume (ml)	Volume (ml)	volume (ml)	-
0.05	20	20	20	50
0.10	20	20	20	50
0.15	20	20	20	50
0.20	20	20	20	50

Different molar concentrations were obtained by preparing them using distilled water. The concentration of copper sulphate was varied from 0.05 M to 0.20 M.

All reagents were poured into 100 ml beaker which was put into a water bath kept at a constant temperature of $\approx 75^0$ C starting with copper sulphate followed by tartaric acid while stirring the solution thiourea is then added. The solution is then stirred for 10 minutes and ammonia solution is added drop wise until the pH of the solution is above 9.5. While the solution is in the water bath maintained at $\approx 75^0$ C, a clean glass substrate is inserted vertically into the solution for 50 minutes. After deposition for 50 minutes, the substrate coated with Cu_2S is rinsed with distilled water and then air dried.

4.4.2 Deposition of Fluorine doped Tin (IV) Oxide (SnO_2: F) thin films

To deposit SnO_2: F, stannous chloride was dissolved in concentrated HCl by heating it at 90^0 C for ten minutes, the resulting solution was diluted with propan-2-ol to form the starting solution. Fluorine doping was achieved by dissolving ammonium fluoride in a double distilled water and then adding it to the starting solution which forms the precursor solution. The quantities of the reagents used to form a precursor solution are as given in table 4.2.

Table 4.2: Quantities of the reagents used in depositing Fluorine doped Tin Oxide (SnO_2: F) thin films.

% of F	$SnCl_2.5H_2O$ Mass(gram)	NH_4F Mass(gram)	HCl Volume(ml)	Propan-2-ol Volume(ml)	Deposition pressure	Deposition time
0	25	0	5	20	$8.50x10^5$Pa	10
2	25	0.5	5	20	$8.50x10^5$Pa	10
4	25	1.0	5	20	$8.50x10^5$Pa	10
6	25	1.5	5	20	$8.50x10^5$Pa	10
8	25	2.0	5	20	$8.50x10^5$Pa	10

To achieve different percentage of fluorine doping, the weight percentages of ammonium fluoride (NH_4F) to stannous chloride ($SnCl_2.5H_2O$) was varied as shown in table 4.2. The percentage of fluorine doping was varied from 0 % to 8 % at intervals of 2 %. The precursor solution was then poured into the spray pyrolysis apparatus, the pressure of the carrier gas was set to about $8.50x10^5$ Pa.

The atomized solution was then sprayed onto a glass substrates which were maintained at a temperature of 350^0 C by the heater for ten minutes. The coated glass substrates were then left to cool on the hot plate for ten minutes and then air dried at room temperature.

4.5 Procedures of Characterization of thin films

4.5.1 Optical Characterization of thin films

UV-VIS-NIR double beam spectrophotometer solid state 3700 machine shown in figure 3.5 in the range of 300 nm – 1200 nm was used to measure reflectance and transmittance of all thin film samples deposited. Transmittance was calculated by equation 4.1;

$$T = \frac{I_t}{I_o}$$

(4.1) where T is transmittance, I_t is transmitted intensity and I_o is incident intensity.

Reflectance of the film samples was calculated using equation 4.2;

$$R = \frac{I_R}{I_o} \times 100$$

(4.2)

where R is reflectance, I_R is reflected intensity and I_o is incident intensity.

Optical spectra of the films were simulated using SCOUT software to obtain optical constants such as refractive index (n), absorption coefficient (α) and band gap (E_g). The following models were used; Drude model, OJL and Tauc Lorentz. Drude was used to adjust plasma frequency, charge carrier density and damping constant since the films have free charge carrier. OJL was used to account for interband transitions

and the parameters varied were gap energy, decay and gamma. Tauc Lorentz was used for crystallinity of the films, damping and resonance frequency were varied. The normalized transmittance data was fitted to simulated spectra to generate the optical constants. The inherent equations which SCOUT software uses to generate the optical constants are given in equations 3.1, 3.4, 3.5 and 3.6 in chapter three.

4.5.2 Electrical characterization of thin films

Electrical characterization of all film samples prepared was done using four point probe shown in figure 3.6 to determine sheet resistivity of the samples. The outer two probes were passed with current and then voltage measured in the inner two probe.

From the four point probe set-up, sheet resistance was measured by passing a DC current through the outer two probes by raising the stage until slight contact was made by the wafer and probe tips. An electrical circuit is completed by this connection which makes a voltage to be induced in the inner two points. The thickness of the films were calculated from simulated data.

Sheet resistivity for thin films were calculated from simulated data using equation 4.3 as derived from equation 3.7 to 3.10 in chapter three.

$$\rho_s = 4.532t\ \frac{V}{I} \qquad (4.3)$$

where $\kappa = \pi/\ln 2 = 4.532$ is a geometric correction factor, V is voltage, I is current and t is film thickness.

4.5.3 Fabrication and characterization of Cu_2S/ SnO_2: F p-n junction.

Cu_2S/SnO_2: F was fabricated in stages. Starting with the n-type layer of SnO_2: F thin films which was deposited onto the glass substrate by spray pyrolysis technique. Then the p-type layer of Cu_2S thin film was deposited onto SnO_2: F thin film on the same glass substrate by CBD method.

The characteristics performance of the solar cell were studied using a solar simulator. A constant monochromatic beam was incident to the cell. The solar simulator was interfaced with Keithley Sourcemeter which recorded current as the voltage across the cell was varied. The data acquisition was computerized. The I-V data obtained was used to plot the current- voltage curve from which the cell performance parameters such as open circuit voltage (V_{oc}), short circuit current (I_{sc}), maximum power (P_{max}), fill factor (ff) and efficiency (η) were calculated using equations 3.11 to 3.16 in chapter three (Markvart, 1998).

CHAPTER FIVE

RESULTS AND DISCUSSION

5.1 Introduction

Figures, tables and graphs are used to present results and analysis of the study. The optical and electrical characteristics of copper sulphide (Cu_2S) p- type and fluorine doped tin oxide (SnO_2: F) n-type thin films are discussed extensively. The current-voltage characteristics of the fabricated cell are also analyzed in this chapter.

5.2 Optical characterization of the films

5.2.1 Transmittance of copper sulphide (Cu_2S)

Figure 5.1 shows transmittance spectra of Cu_2S thin films deposited at varying concentration of $CuSO_4$ against wavelength in the range of 300 nm to 900 nm.

The curves show low transmittance below 40 % for all the samples across the entire wavelength. The maximum transmittance was observed at approximately 780 nm wavelength for all the samples. Ezema *et al*. (2006) obtained a comparable result with transmittance of 47%. Therefore, Cu_2S thin film has a low transmittance at shorter wavelengths below 780 nm making them appropriate in applications as absorber layer

in solar cells due to their fundamental absorption lying within the range of solar cell operation (visible range).

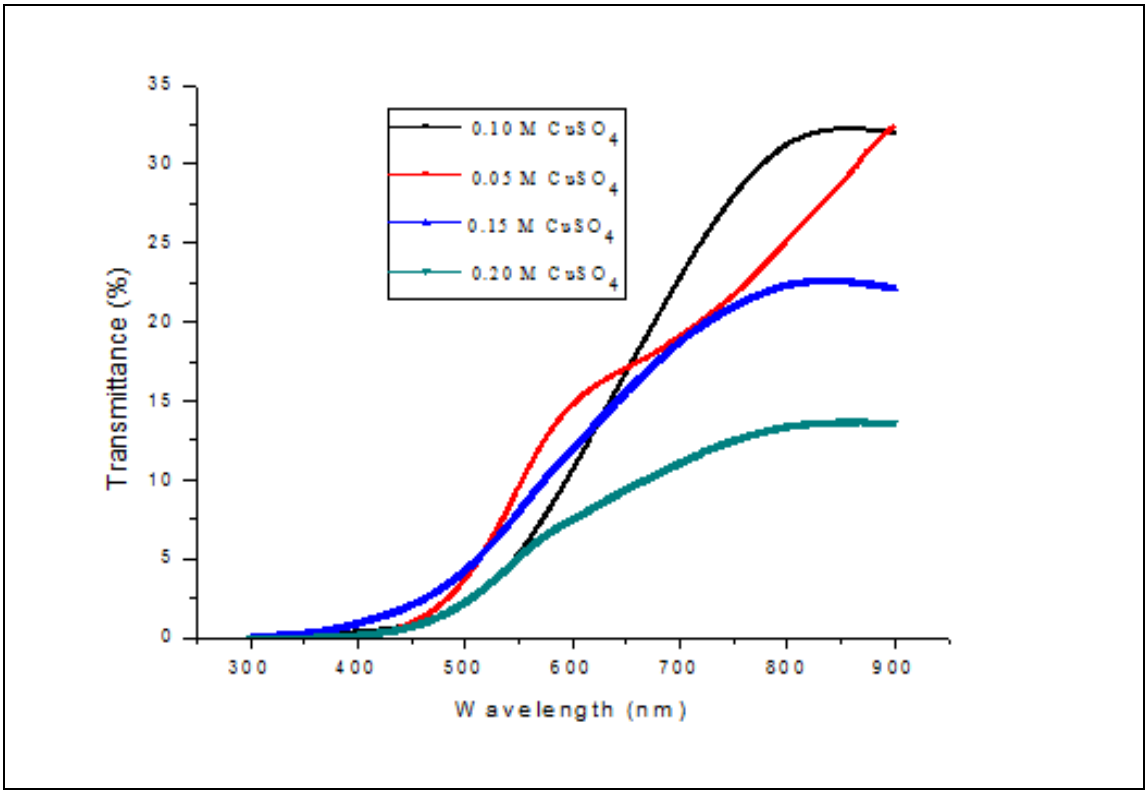

Fig. 5.1: Variation of transmittance (T) with wavelength (λ) for Cu_2S thin films deposited at varying precursor concentration.

Table 5.1: Average transmittance (%) in visible region for varying Cu^{2+} concentration

Concentration of Cu^{2+}	0.05 M	0.10 M	0.15 M	0.20 M
Average transmittance in VIS (%)	33.48	32.96	20.91	16.46

From table 5.1, at lower concentrations of copper (0.05 M and 0.10 M), transmittance is higher compared to higher copper concentrations (0.15 M and 0.20 M) which gives low transmittance.0.15 M copper concentration was found to the optimum

concentration to deposit copper sulphide thin films as a p-type layer for solar cell application due to its low transmittance and high conductivity.

5.2.2 Reflectance of Cu_2S thin films

Figure 5.2 shows reflectance of copper sulphide films (Cu_2S) in the range of 300 nm to 900 nm.

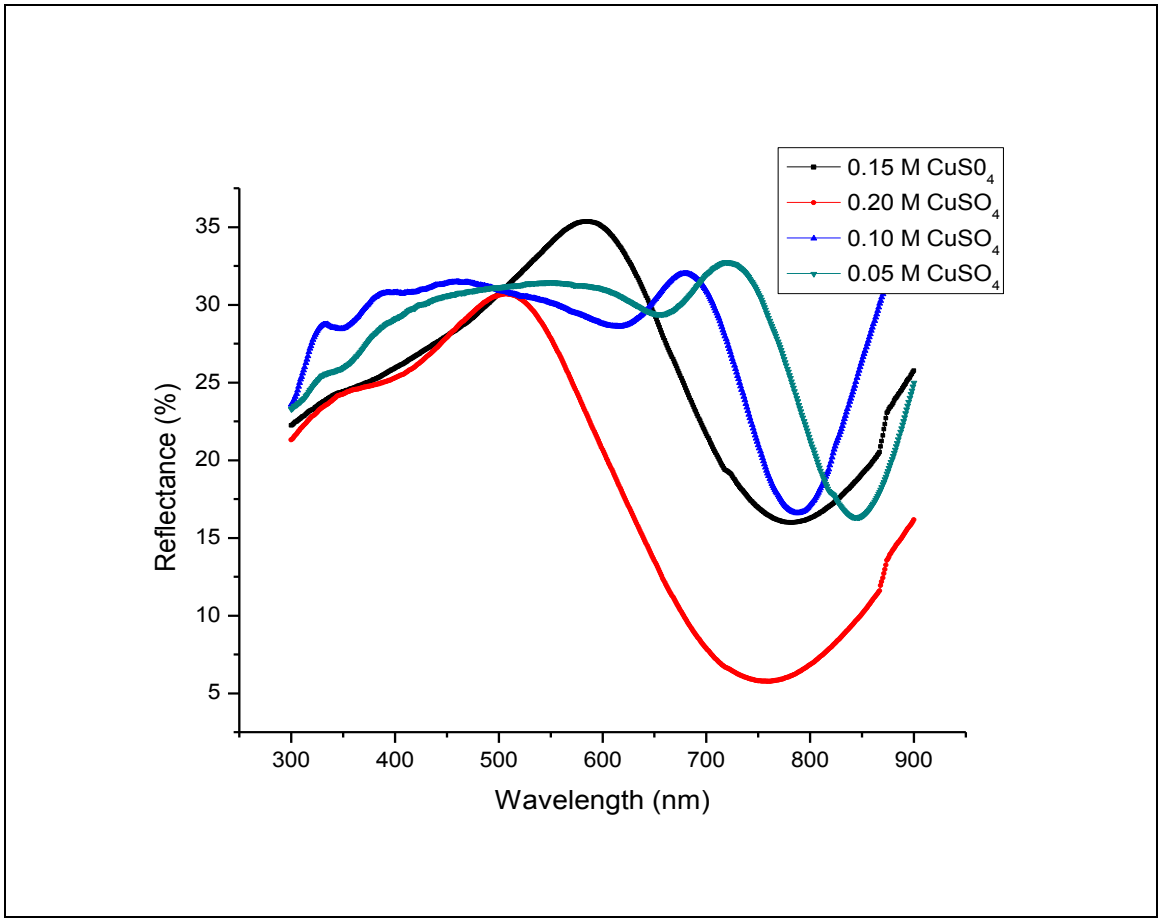

Fig. 5.2: Reflectance (R) against Wavelength (λ) for copper sulphide thin films (Cu_2S) deposited at varying precursor concentration.

From figure 5.2 above, copper sulphide thin films deposited at low copper concentration (0.05 M and 0.10 M) have higher reflectance than those deposited at a high copper concentration (0.15 M and 0.20 M). From the curves, reflectance for all the samples is below 37 %. Cu_2S thin film deposited at 0.15 M copper concentration with average reflectance of 27.8 % was selected for optimization. The reflectance

spectra of copper sulphide thin films shows low percentage reflectance making Cu_2S thin film suitable material for application as an absorber layer (p-type) in solar cells.

5.2.3 Absorbance of Cu_2S thin films

Cu_2S thin film has relatively higher absorbance and the absorbance increases with increase in the copper concentration (Kumar *et al.,* 2013). From figure 5.3, Cu_2S thin film deposited at 0.15 M concentration of copper had the highest absorbance (above 50 %) between 380 nm to 650 nm.

Table 5.2: Average absorbance (%) in visible region for different copper concentration

Concentration of Cu^{2+}	0.05 M	0.10 M	0.15 M	0.20 M
Average absorbance in VIS (%)	31.52	33.04	51.29	49.93

Absorbance of Cu_2S increases with concentration of copper, this is associated to an increase in the thickness which results in an increase in the depth of donor level available for photons to be absorbed (Abbas *et al.,* 2015).

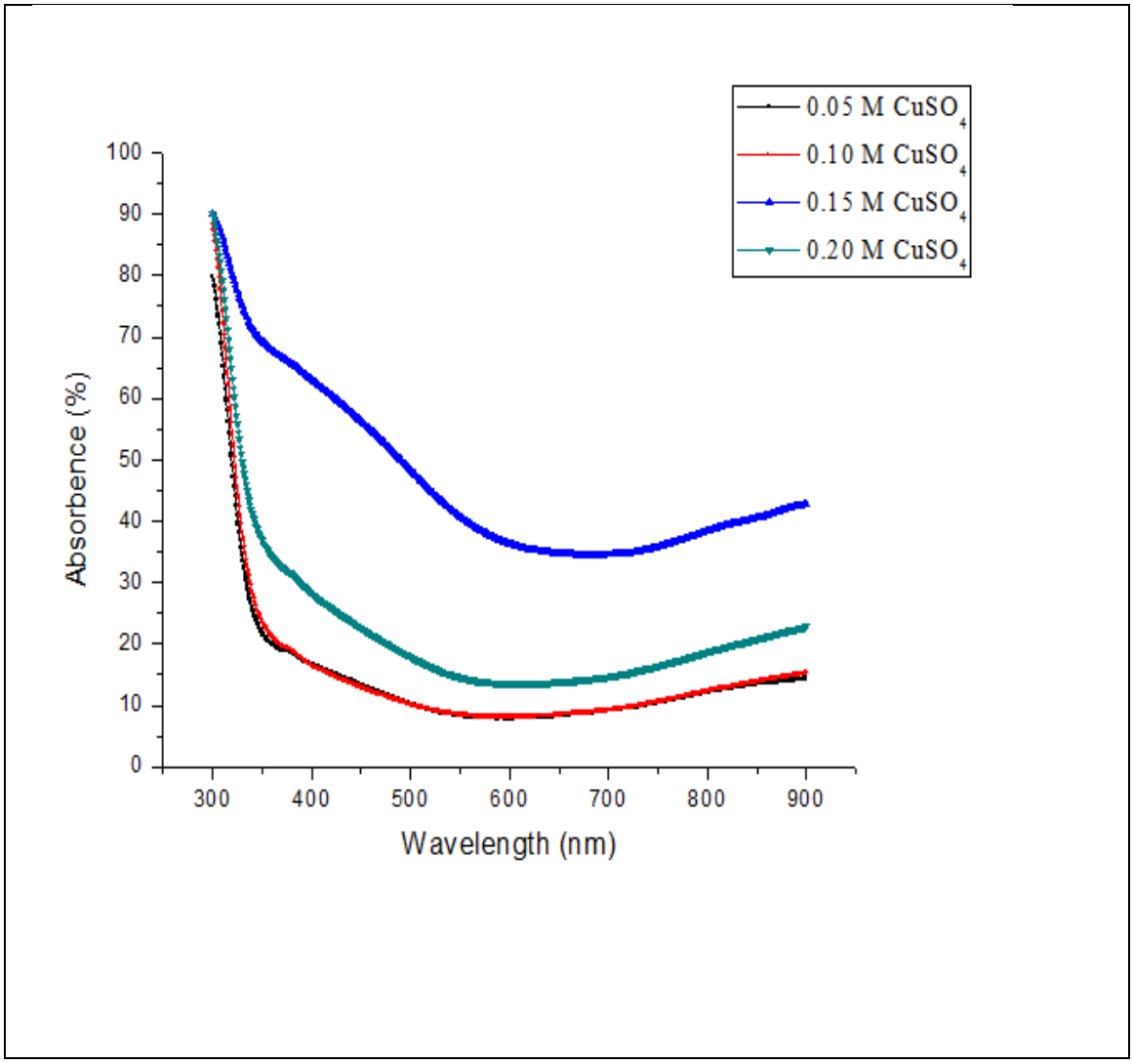

Fig. 5.3: Absorbance (A) against Wavelength (λ) for copper sulphide thin films (Cu_2S) deposited at varying Cu^{2+} concentration.

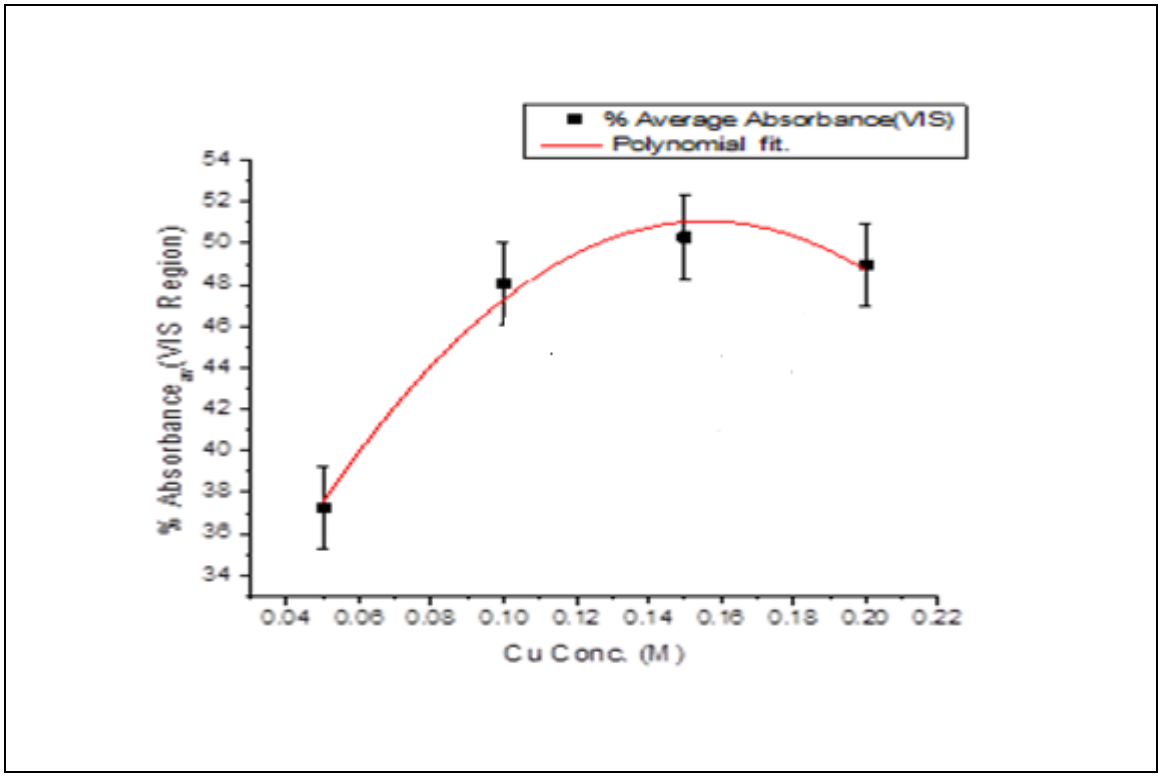

Fig. 5.4: Polynomial fit for average absorbance of Cu2S deposited at varying precursor concentration

5.2.4 Band gap of Cu_2S

The direct optical band gap, E_g of Cu_2S thin films were determined using equation 3.6

(Ogwu *et al*., 2007).

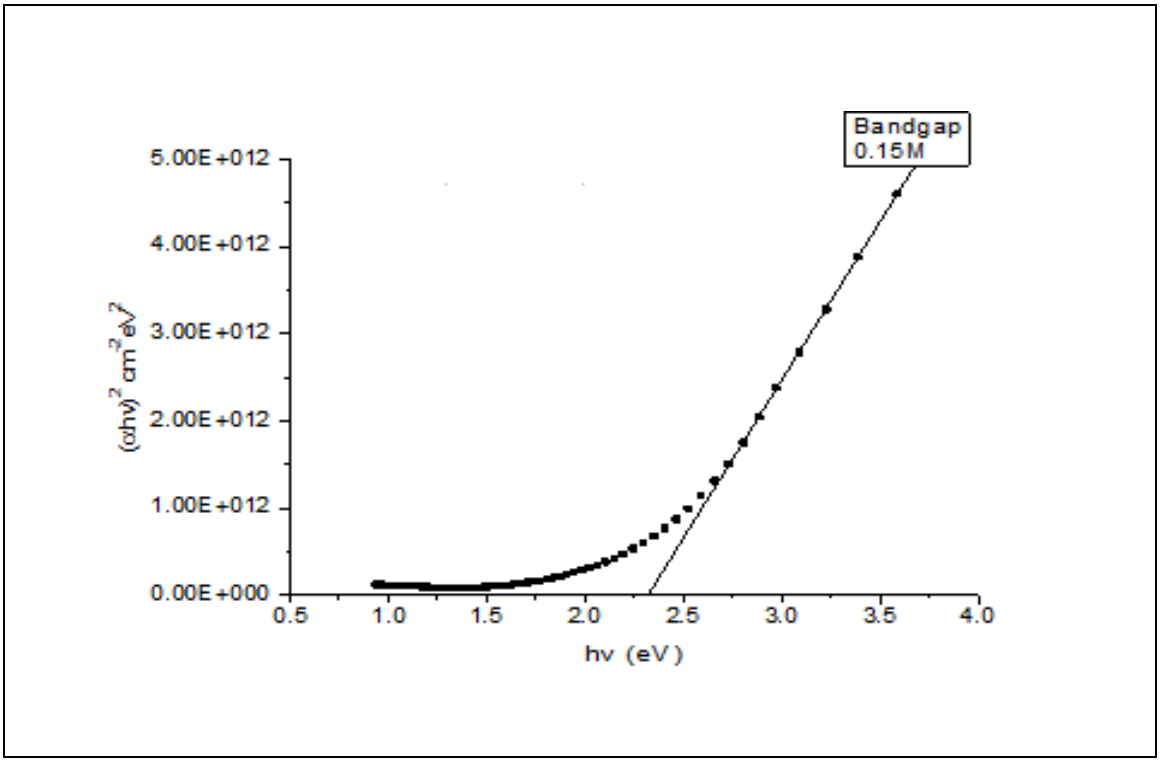

Fig. 5.5: A graph of $(\alpha h\nu)^2$ verses $h\nu$ (photon energy) for Cu_2S

The values of the band gap obtained by using the graph in figure 5.5 for Cu_2S thin films of different concentrations of copper were compared to the values obtained from simulation as shown by table 5.3.

Table 5.3: Band gap energy of Cu_2S thin film for different copper concentration.

Concentration of Cu^{2+}	Calculated band gap (Eg) (eV)	Simulated band gap (Eg) (eV)	Film thickness (t) (nm)
0.05 M	2.41	2.42	146.3
0.10 M	2.39	2.41	167.7
0.15 M	2.33	2.35	195.5
0.20 M	2.34	2.37	197.3

The band gap energy obtained varies between 2.33 eV to 2.42 eV, this in agreement with the results obtained by others on the same material. Cu_2S thin film has a direct band gap ranging between 2.46 eV to 3.1 eV (Luminita *et al.,* 2009). Cu_2S thin film deposited by spray pyrolysis technique is a p-type material with a direct band gap energy ranging between 1.2 eV to 2.4 eV (Ahirrao *et al.*, 2014).

The results in table 5.3 show that Cu_2S is a narrow band gap material which is suitable for application as an absorber layer in solar cells. 0.15 M copper concentration is the optimum concentration for deposition of Cu_2S since Cu_2S deposited at that concentration has the least band gap energy of 2.33 eV.

5.2.5 Refractive index of Cu_2S

Figure 5.6 shows a graph of average refractive index against concentration of copper ions. From this figure, it can be observed that the minimum average refractive index is 1.44. The concentration of Cu^{2+} increases film cryatallinity of Cu_2S.

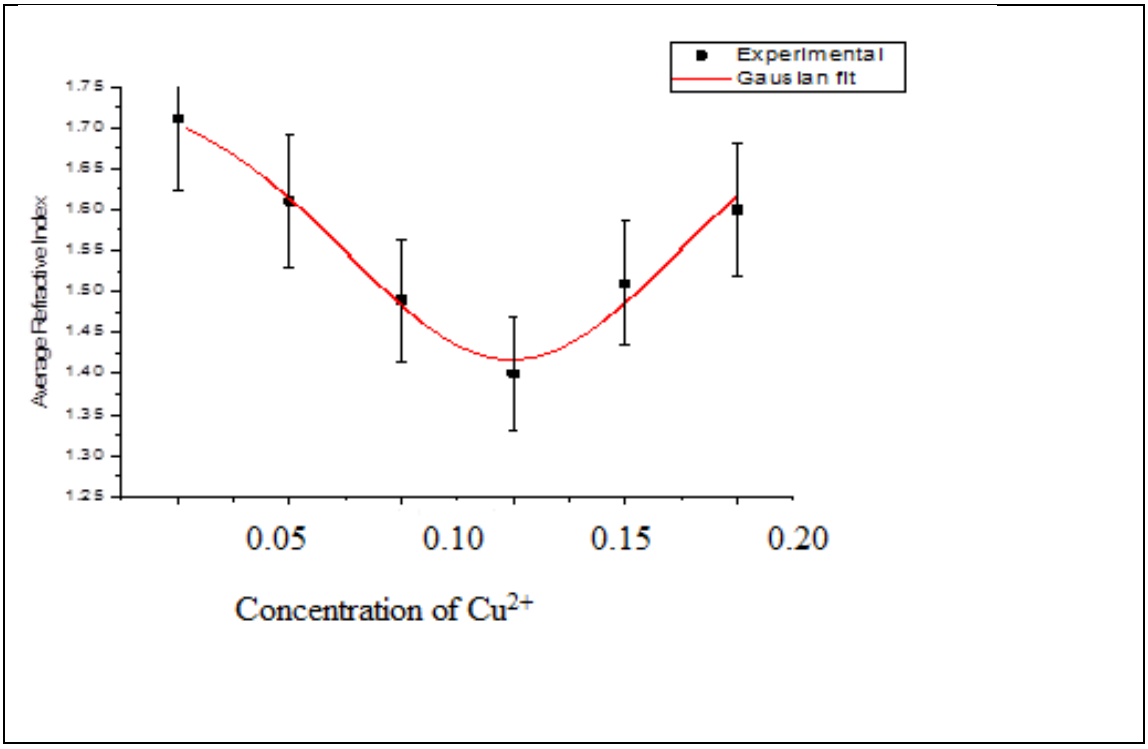

Fig. 5.6: A graph of refractive index against copper ion concentration

5.3 Electrical characterization of Cu_2S films

Resistivity for thin films deposited at varying copper concentration ranging from 0.05 M to 0.20 M were measured and conductivity for each sample was calculated as shown in table 5.4.

Table 5.4: Variation of sheet resistivity with copper concentration for Cu_2S thin films

Concentration of Cu^{2}+ (M)	Resistivity (ρ)x10^{1} (Ω cm)	Conductivity (σ) (Ω cm)$^{-1}$	Film thickness (t)(nm)
0.05	17.24	0.0058	146.3
0.10	5.95	0.0168	167.7
0.15	0.40	0.2500	195.5
0.20	0.42	0.2380	197.3

A concentration of 0.15 M gave the lowest resistivity (0.40 x10^{1}Ω-cm) and was chosen as the optimal concentration for deposition of Cu_2S as an absorber layer for solar cells applications. From the results obtained, resistivity decreases with an increase in copper ions (Cu^{2+}). Resistivity of Cu_2S decreases as the copper ions increase and this is due to an increase in mobility and carrier concentration (Fayroz *et al.*, 2016).

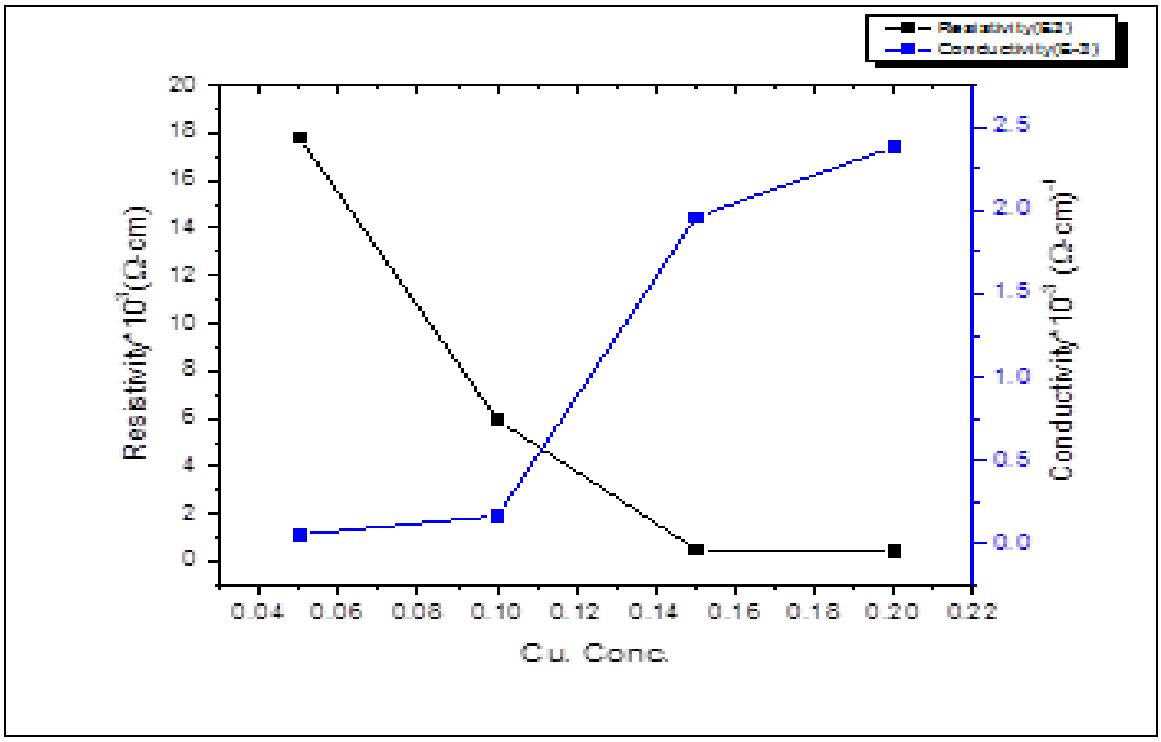

Fig. 5.7: A graph of variation of resistivity and conductivity with Cu^{2+}concentration for Cu_2S.

The electrical resistivity of Cu_2S thin film decreases as the thin film thickness increases this was in agreement when compared to other research done on the same material. The decrease of sheet resistivity of Cu_2S thin film with increase in thickness

is associated with the increase in the size of the grain and carrier concentration of Cu^{2+} (Ramya and Ganesan, 2011).

5.4 Optical characterization of SnO_2: F thin films

5.4.1 Transmittance of SnO_2: F thin films

Transmittance curves of SnO_2: F thin films in figure 5.8 shows that transmittance of SnO_2: F thin films is high (above 75 %) for all the samples. Comparable result obtained by Sumanta *et al*. (2012) indicates that transmittance of SnO_2: F is above 70 %. Elangovan and Ramamurthi (2016) reported on SnO_2: F having the highest transmittance of 85 % at 800 nm wavelength.

From figure 5.8, it observed that optical transmittance decreases as the fluorine concentration increases. Yousaf *et al*. (2008) also indicated that transmittance of SnO_2: F thin films decreases as the concentration of fluorine increases and this is attributed to an increase in the fundamental absorption resulting from increased carrier concentration as photon striking increases. 4 % fluorine concentration has high transmittance of 79.94 % in visible region and it has a large band gap and therefore chosen as a window layer for solar cells application.

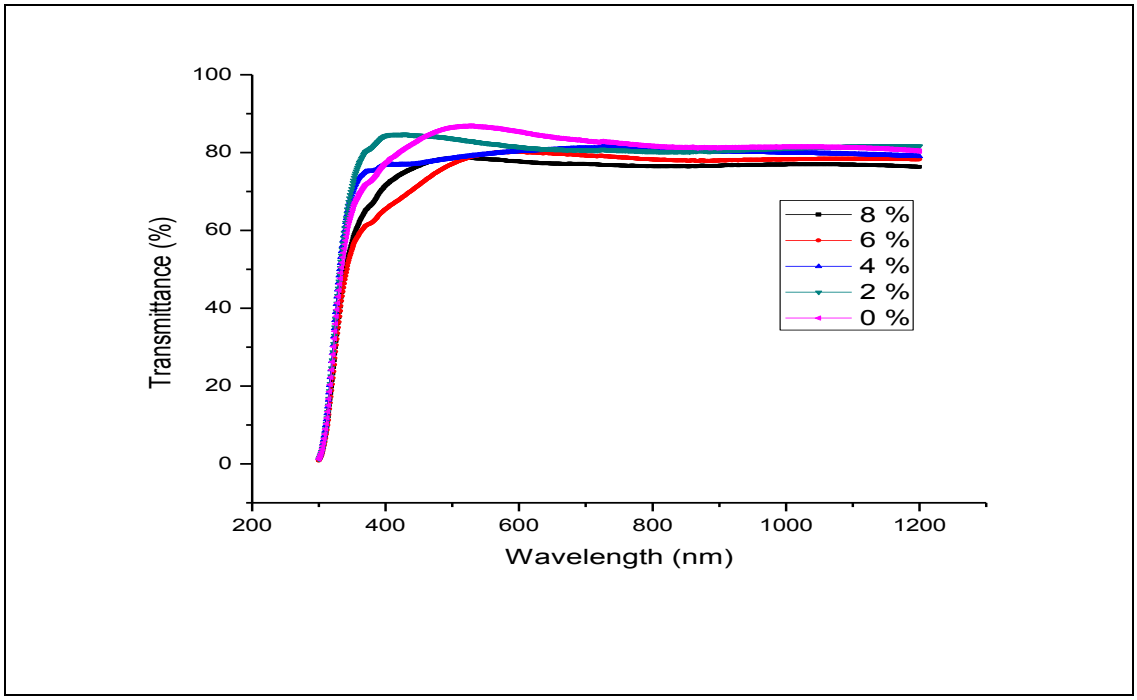

Fig. 5.8: Variation of transmittance against wavelength for SnO_2: F thin films at varying fluorine concentration

Table 5.5: Transmittance (%) of SnO_2: F thin films in visible region for different fluorine doping percentages.

Fluorine doping (%)	0	2	4	6	8
Average transmittance in VIS (%)	84.10	82.29	79.94	77.52	77.28

5.4.2 Reflectance of SnO_2: F thin films

Figure 5.9 shows reflectance spectra of SnO_2: F thin films as a function of fluorine doping %. From the graph, all the thin film samples have average reflectance values

below 16 % in the visible range. Hassanien et *al*. (2016) reported reflectance of about 12 % between 500 nm to 1500 nm. From the study, reflectance was generally low making SnO_2: F thin films suitable in solar cells applications as window layers. The spectra behavior of SnO_2: F thin films shows reflectivity which is smooth on the surface hence less surface scattering loss (Osoro, 2011)

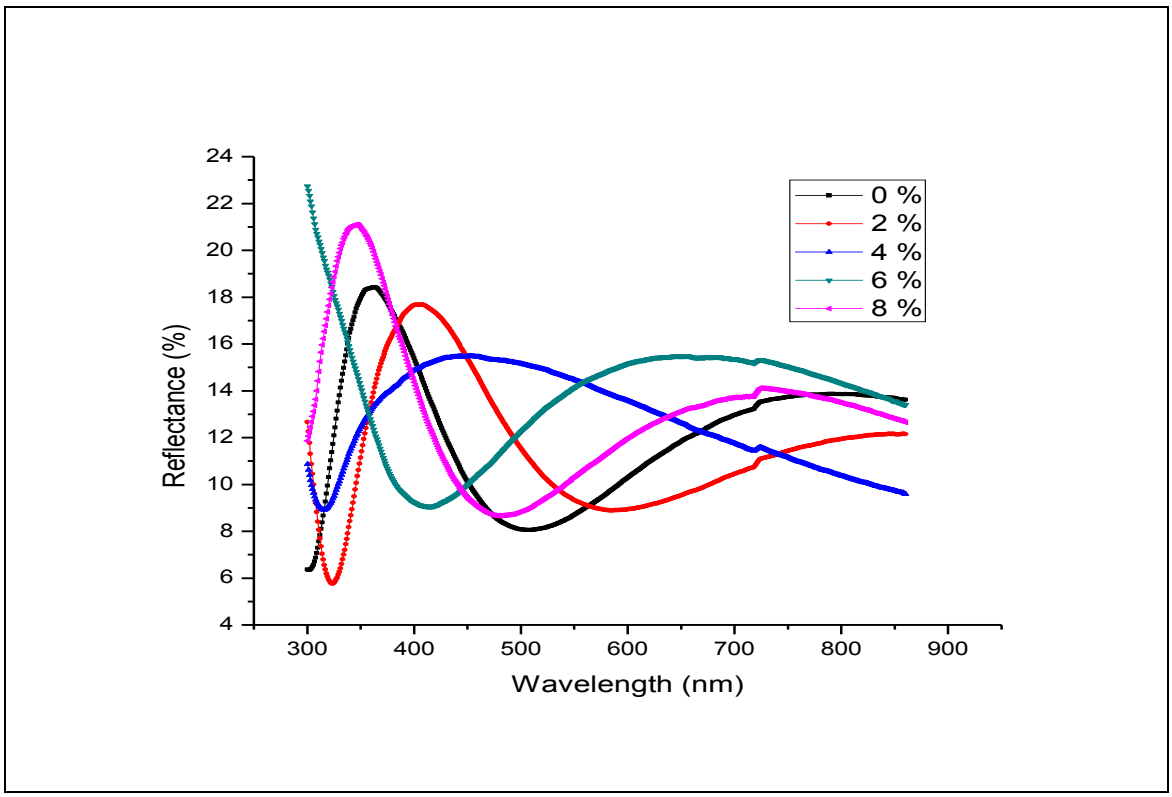

Fig. 5.9: Graphs of variation of Reflectance against wavelength for SnO_2: F thin films at varying fluorine concentration.

5.4.3 Absorbance of SnO_2: F thin films

The absorbance spectra of SnO_2: F in figure 5.10 shows that the average absorbance of SnO_2: F thin films is below 20 % in the range of 400 nm to 1200 nm wavelength. This result confirms that SnO_2: F is an n-type semiconductor and a poor absorber of

solar radiation. This is in conformity with the properties of a window layer in solar cells applications (Banerjee *et al.*, 2003)

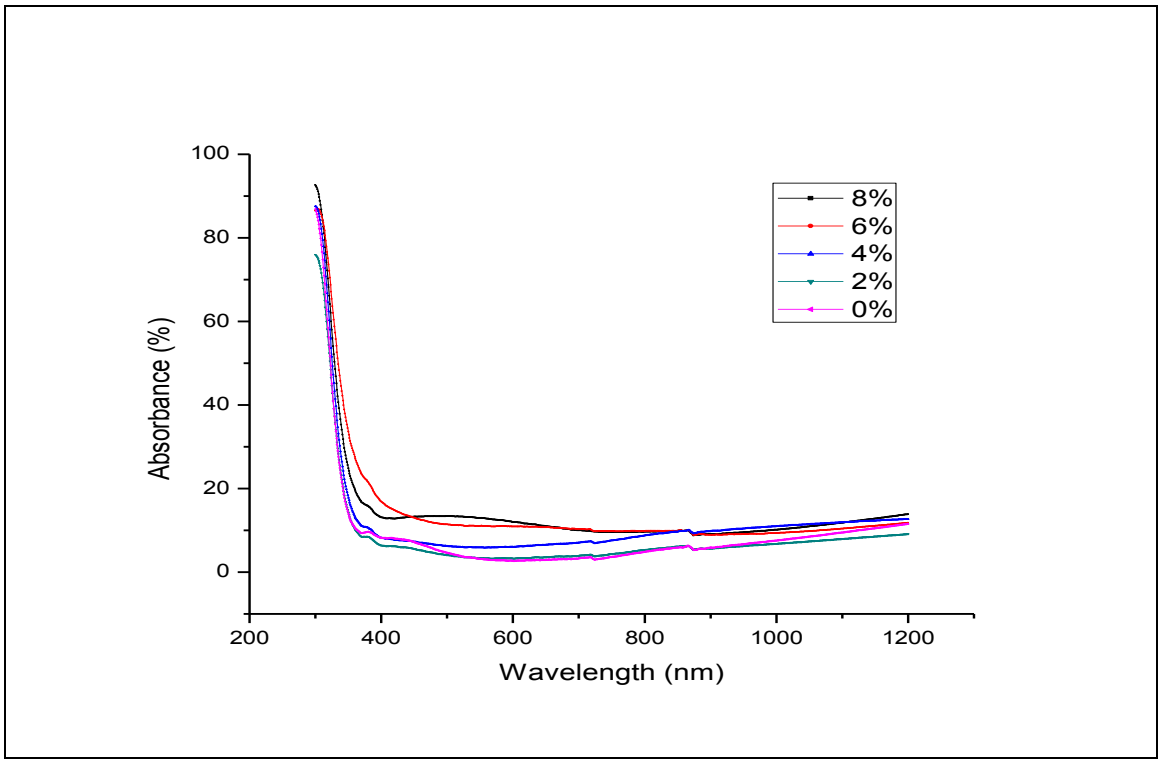

Fig. 5.10: Variation of Absorbance with λ for F: SnO_2 thin films at varying fluorine concentration

5.4.4 Band gap energy of SnO_2: F

Figure 5.11 shows band gap energy (E_g) of SnO_2: F thin films at 4 % fluorine doping.

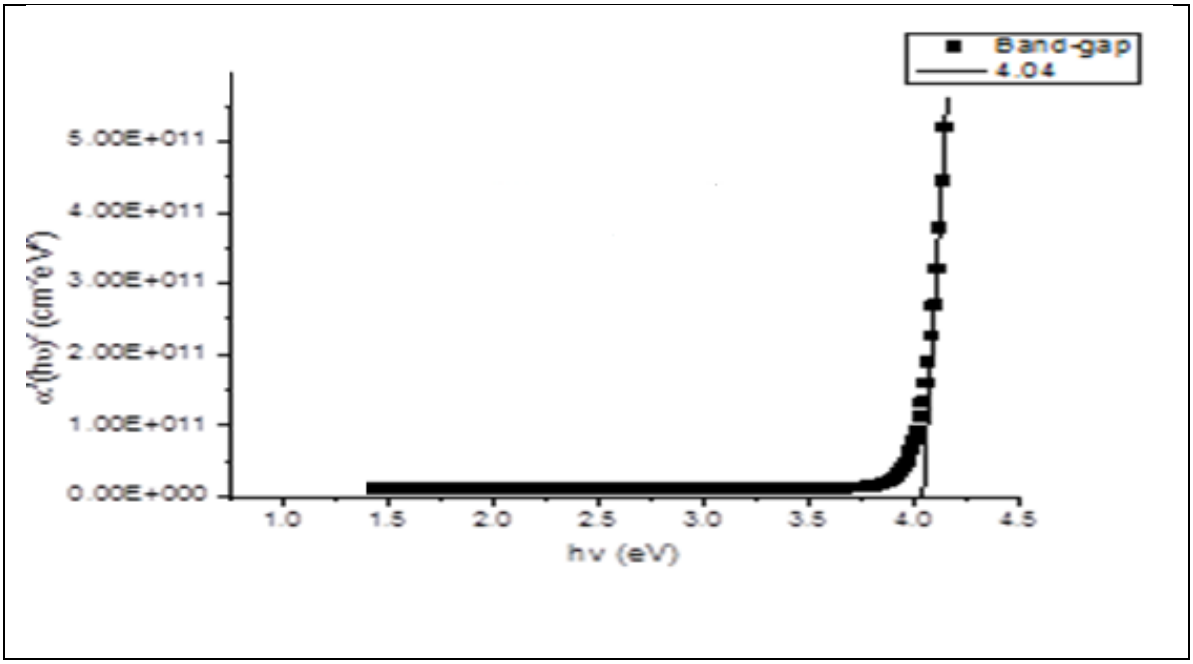

Fig. 5.11: A graph of $(\alpha h\nu)^2$ verses $h\nu$ (photon energy) for SnO_2:F at 4 % fluorine doping

Table 5.6 shows the band gap energy for different fluorine doping concentrations ranging from 0 % to 8 %.

Table 5.6: Band gap energy of SnO_2: F thin films for different fluorine doping percentages

Fluorine doping %	0	2	4	6	8
Calculated E_g	3.92	3.97	4.04	4.04	4.06
Simulated E_g	3.95	3.99	4.05	4.05	4.07

The values of the band gap in table 5.6 show that SnO_2: F films have a wide energy gap (E_g) ranging from 3.92 eV to 4.06 eV for fluorine doping percentages 0 % to 8 %

respectively. The band gap energy increases as the fluorine doping percent increases (Mosiori *et al.*, 2017).

This result is in conformity with the one obtained by Moholkar *et al.* (2009) which shows that the band gap energy of SnO_2: F increases with increase in fluorine doping up to 20 wt. % of NH_4F. This is attributed to the increase in carrier concentration of the n-type which drift to higher energy levels of the absorption edge (Banerjee *et al.*, 2003). 4 % fluorine doping was chosen as the optimum percent for deposition of SnO_2: F thin film since SnO_2: F deposited at 4 % fluorine doping had the highest band gap energy of 4.04 eV.

5.4.5 Refractive index of SnO_2: F

From figure 5.12, it is observed that refractive index increases with fluorine doping. Refractive index increases with concentration because presence of a dopant enhances transparent of deposited thin films. In addition, improved crystallinity increases the refractive index of the film.

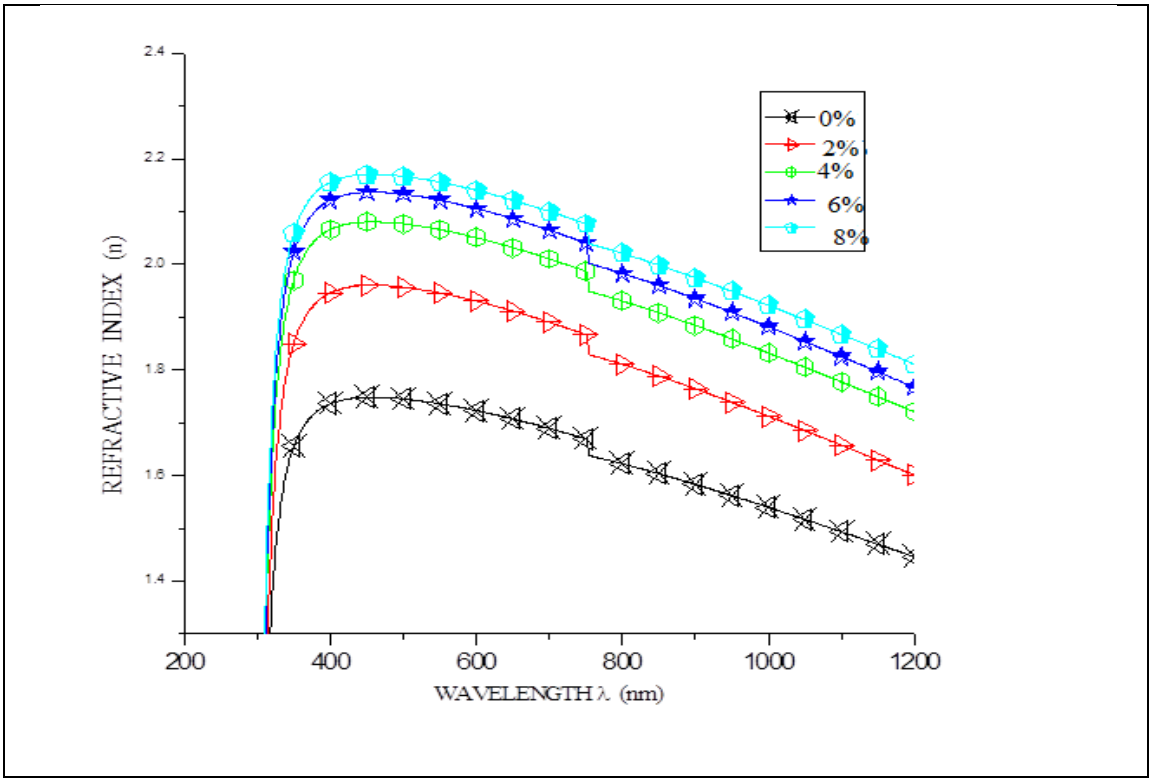

Fig. 5.12: Refractive index against wavelength for SnO_2: F at varying fluorine concentration

5.5 Electrical characterization of F: SnO2 films

The obtained results were tabulated in table 5.7. The resistivity of the thin films decreases with increase of fluorine doping concentration. 4 % fluorine doping concentration had the lowest resistivity value of 4.026 x 10^1 Ω-cm. Electrical resistance of SnO_2: F thin films decreases with increase in fluorine concentration due to an increase in the number of charge carrier (Takanoglu *et al.*, 2015). Further increase in fluorine concentration above 4 % resistivity starts to increase. This is consistent with the result obtained by Moholkar *et al*. (2009) having minimum resistivity of $3.8x10^{-4}$ at 20 % wt. of NH_4F and the increase in resistivity of the thin films when fluorine concentration is increased above 20 % NH_4F is attributed to

decreased mobility caused by disorientation of the structure of the thin films (Mosiori and Oeba, 2017).

Table 5.7: Variation of sheet resistivity with fluorine doping concentration for SnO_2: F thin films

Fluorine doping (%)	Resistivity(ρ)x10^{+1}(Ω cm)	Conductivity (σ) (Ω cm)$^{-1}$
0	45.65	0.0022
2	38.99	0.0026
4	4.03	0.0250
6	5.86	0.0171
8	7.38	0.0140

Figure 5.13 shows a graph of sheet resistivity and conductivity as a function of fluorine doping concentration. It is observed that conductivity increases as sheet resistivity decreases with increasing fluorine concentration. Above 4 % fluorine doping, sheet resistivity of the thin films starts to increase as conductivity of the films decreases.

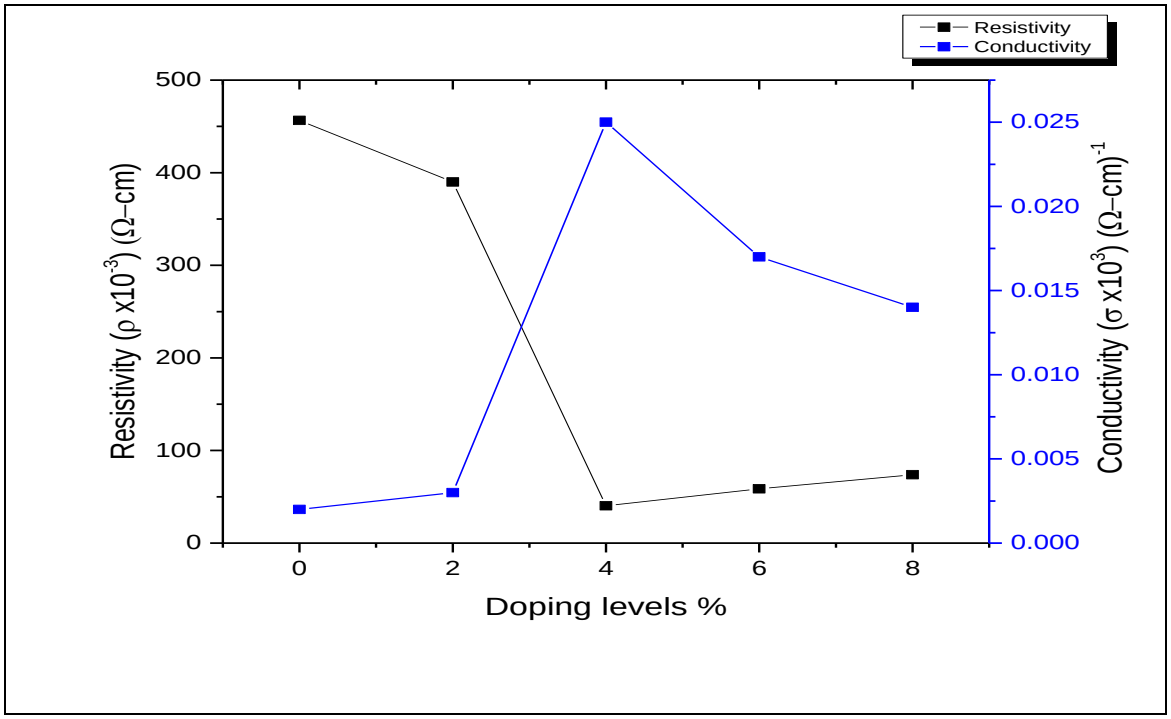

Fig. 5.13: Graphs of resistivity and conductivity as a function of fluorine conc.

5.6 Optimized Opto-electric parameters for cell fabrication

5.6.1 p-type absorber layer (Cu_2S) thin films

0.15 M concentration of copper sulphate($CuSO_4$) was chosen as the optimum concentration of Cu^{2+} because the films deposited with this concentration had the highest absorbance (51.29 %), narrow band gap energy (2.33 eV) and low resistivity of 0.40×10^3 Ω-cm making the thin film deposited at this concentration a suitable absorber for solar cells applications.

5.6.2 n-type window layer (SnO_2: F) thin films.

SnO_2: F thin films deposited at 4 % fluorine doping gave the high transmittance (79.94 %), wide band gap energy (4.04 eV) and low sheet resistivity of 40.26 Ω-cm

and therefore was chosen as the optimum concentration of fluorine for deposition of SnO_2: F thin films as window layers for fabrication of p-n solar cells.

5.7 Current- Voltage Characterization of the solar cell.

Table 5.8 gives current (I), voltage (V), current density (J) and power (P) for Cu_2S/SnO_2: F p-n junction solar cell. The active area (A_c) of the fabricated cell was 1.8 cm x 1 cm (0.00018 m^2)

Table 5.8: Current, Voltage and Power characteristics of the p-n junction solar cell.

Voltage(V) ±0.00005	Current, I (A) ±0.000005	Current density, J (A/cm^2) ±0.000005	Power(W) ±0.000005
0.4075	0	0	0
0.3675	0.00093	0.00051	0.00034
0.3275	0.00145	0.00081	0.00045
0.2875	0.00187	0.00104	0.00055
0.2475	0.00199	0.00111	0.00049
0.2075	0.00209	0.00116	0.00043
0.1675	0.00214	0.00119	0.00036
0.1275	0.00217	0.00121	0.00028
0.0875	0.00218	0.00121	0.00019
0.0475	0.00218	0.00121	0.00010
0.0075	0.00219	0.00122	0.00002
0	0.00219	0.00122	0

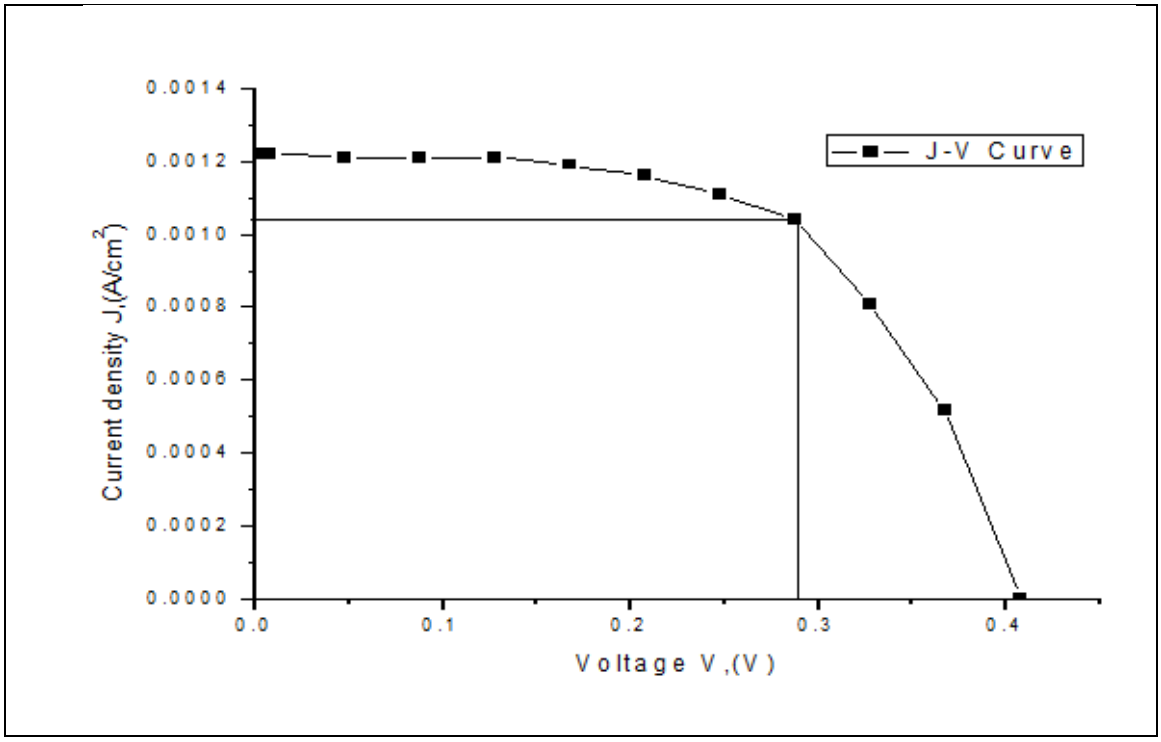

Fig. 5.14: J-V Curve in terms of current density at 1000 W/m^2 intensity.

The active area (A_c) of the solar cell is 1.8 cm by 1 cm (0.00018 m^2) and incident radiation (E) was 1000 W/m^2. From figure 5.14, the fabricated solar cell has open circuit voltage (V_{oc}) of 0.4075 V and short circuit current density (J_{sc}) of 0.001219 A/cm^2. Comparable results by Fukuda and Ichimura (2013) obtained V_{oc} = 0.29 V, I_{sc} = 0.58 Ma/cm^2 and FF = 0.30 when using Cu_2S as an absorber layer on fabrication of TiO/Cu_2S solar cells.

Figure 5.15 a graph of current, voltage and power for the fabricated cell when illuminated by a solar simulator. The fill factor (FF) and conversion efficiency (η) of Cu_2S/SnO_2: F p-n junction solar cell were determined using equations (3.15) and (3.16) respectively. The cell had a fill factor (FF= 0.61) and conversion efficiency (η = 0.303 %). The low values of current and power were obtained due to recombination of charges at the junction and high series resistance.

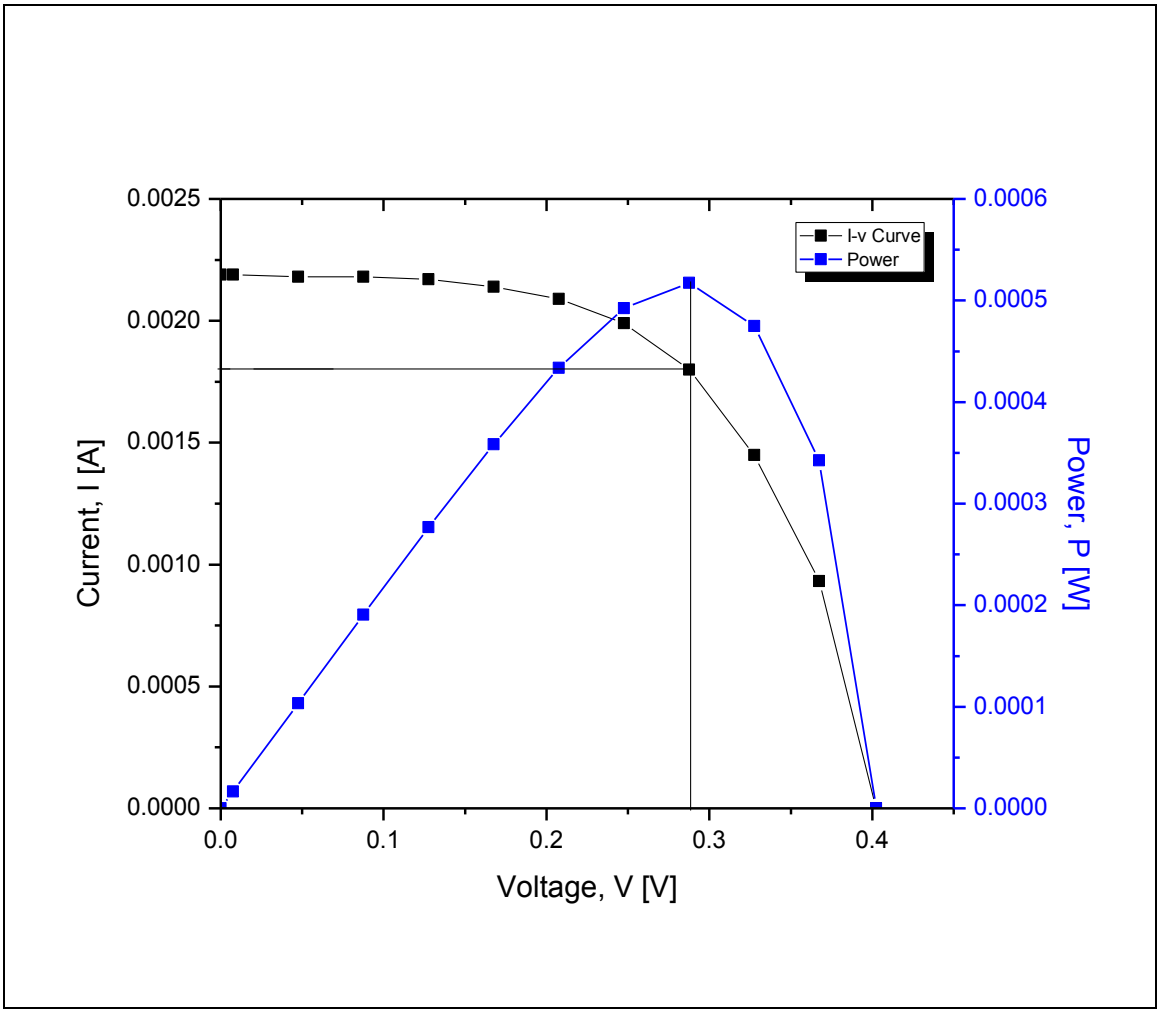

Fig. 5.15: Current-Voltage and power curves for Cu_2S/SnO_2: F p-n junction solar cell.

Table 5.9: Summary of the p-n junction solar cell parameters

Cell parameter	I_{sc} (A)	V_{oc} (V)	V_{max} (V)	I_{max} (A)	P_{max} (W)	FF	η
Value parameter	0.00219 A	0.4075 V	0.29113 V	0.00187 A	0.00055 W	0.61	0.303%

The cell has open circuit voltage of (V_{oc}= 0.4075 V), short circuit current of (I_{sc}= 0.00219 A). The maximum current (I_{max}) and maximum voltage (V_{max}) were 0.00187 A and 0.29113 V respectively. The maximum power (P_{max}) of the cell was 0.00055W. The fill factor and efficiency of the cell were 0.61 and 0.303 % respectively.

CHAPTER SIX

CONCLUSIONS AND RECOMMENDATIONS

6.1 Conclusions

The thin films of copper sulphide (Cu_2S) and fluorine doped tin oxide (SnO_2: F) were successfully deposited by chemical bath deposition method and spray pyrolysis technique respectively. The transmittance of SnO_2: F was 79.94 % in the visible range of the solar spectrum. The reflectance and absorbance of the thin films are below 16 % and 20 % respectively. Making it suitable in solar cells applications as a window layer. 0.15 M copper sulphate ($CuSO_4$) was found to be the optimum concentration for deposition of Cu_2S thin films. The films deposited at this concentration gave the highest absorbance (51.29 %). SnO_2: F thin films deposited at 4 % fluorine doping had a wide band gap of 4.04 eV which is appropriate for a window material while the band gap of Cu_2S was 2.33 eV showing that Cu_2S is an absorber material.

Electrical properties of SnO_2: F and Cu_2S thin films show that resistivity of the films decreases with increase in fluorine and copper concentrations respectively. SnO_2: F has the lowest resistivity of 40.26 Ω-cm at 4 % fluorine doping while Cu_2S has the lowest resistivity of 4.00 Ω-cm at 0.15 M copper concentration.

The fabricated solar cell (Cu_2S/SnO_2: F) has open circuit voltage (V_{oc} = 0.4075 V), short circuit current (I_{sc}= 0.00219 A), maximum voltage (V_{max}= 0.29113 V), maximum current (I_{ma} = 0.00187 A), maximum power (P_{ma} = 0.00055 W), fill factor (FF = 0.61) and efficiency (η = 0.303 %).

The low value of conversion efficiency obtained is attributed to high series resistance due to metal contacts and impurities in the concentrations used in depositing the thin films. High recombination of charge carriers of Cu_2S also affects the efficiency of the cell.

6.2 Recommendations

Based on the low efficiency achieved; other film deposition techniques should be tried and their efficiency be compared with CBD and Spray pyrolysis on Cu_2S/SnO_2: F p-n junction solar cells. A buffer layer be created in the junction to maximize generation and minimize recombination effect which lowers the short circuit current and reduces open circuit voltage hence lowering efficiency of the cell and also further research to be carried out to investigate how use of appropriate antireflective coating which will minimize reflection of the incident radiation and enhance absorption of photon energy will improve the efficiency of Cu_2S/SnO_2: F solar cell.

REFERENCE

Abbas N.K. and Ghdeed N. J. (2015). Effects of thickness on optical properties of Cu_2S thin films. *Iraq Journal of Physics* **13**:26:121-127

Ahirrao P.B., Gosavi S.R., Patil D.R., Shinde M.S. and Patil R.S. (2014). Photoluminescence properties of modified chemical bath deposited copper oxide thin film. *Archives of Applied Science Research* **3:**288-291

Ashour, A. (2006). *The physical characteristics of Cu_2S/CdS thin-film solar Cell*. Journal of Optoelectronics and Advanced Materials, **8:** 1447 – 1451.

Banerjee A.N., Kundoo S., Saha P. and Chatto K.K. (2003). Synthesis and characterization o nanocrystalline fluorine doped tin oxide thin films by sol-gel method. *Journal of Sol-Gel Science Technology* **28**:1:105-110

Brown, M. and Jakeman, F. (1996). Theory of four point probe technique as applied to film layers on conducting substrates. *British Journal of applied Physics.* **17**: 1146-1149.

Dzhafarov Y. L., Pathan T. W. and Staffner T.J. (2006), Optical Properties and band offsets of CdS/CuS super lattice. *The pacific journal of Science and Technology* **11**:404 – 407.

Ebrahimias S., Yunus W.Z.W., Kassim A. and Zainal Z. (2011).Synthesis of nanocrystalline SnO_x (x=1-2) thin film using a chemical bath deposition method with improved deposition time, temperature and pH. (http://www.mdpi.com/journal/sensors, accessed 6th Oct 2014) **11**:9207-9216

Ehtenshamul K.A.S.M., Tahmid B.Q. and Mohammad T. F. (2013). Study of efficiency dependence on alloy composition in an $Al_xGa_{I-x}As/Al_xIn_{I-x}As$ hetoro-junction solar cell, an ultra-thin approach international. *Journal of computer application **0975**:8887*.

Elangovan E. and Ramamurthi K. (2003). Optoelectronic properties of spray deposited SnO_2: F thin films for window materials in solar cells. *Journal of Optoelectronic and Advanced Materials* **5**:1:45-54

Ezema F.I., Hide D.D., Ezugwu S.C., Osuji R.U. and Asogwa P.U. (2010). Optical properties of CdS/CuS and CuS/CdS heterojunction thin films deposited by chemical bath deposition technique. *Journal of Ovonic Research* **6**:3:99-104

Ezema F. I., Nnabuchi M. N. and Osuji R. U. (2006). Optical properties of CuS thin film deposited by cbd. *Trends in Applied Science Research* **1**:5:467-476

Fayroz A.S., Naser M.A., Ahmed Z.H. and Hiba S.R. (2016). *CuS p-type thin film characterization deposited on Ti, ITO and glass substrates using spray pyrolysis deposition (SPD) for light emitting diode (LED) applications*. American Institute of Physics

Guoshi J., Wang N., Gong L. and Xuening F. (2004). Optical Properties and Forming Mechanisms of CdZnS thin film grown by chemical bath deposition. *Chalcogenide letters* **7**:349-355.

Gutierrez P.M., Haiyong L. and Jeffrey P. (2002). Thin film surface resistivity. Thesis for experimental methods in material engineering.

Hani Khallaf, Isaiah O. Oladeji, Guangyu Chai, Lee C. (2008). Characterization of CdS thin films grown by chemical bath deposition using four different cadmium sources. *Thin Solid Films* **516:** 7306–7312

Hassanien A.E., Hashem H.M., Moustafa A.M., Hammam M. and Ramadan A.A. (2016). Performance of transparent conducting fluorine doped tin oxide for application in energy efficient devices. *International Journal of Thin Films Science and Technology* **5**:1:55-65

Ichimura M. and Fukuda K. (2013). Fabrication of TiO_2/Cu_2S heterojunction solar cells by electrophoretic deposition and electrodeposition. *Journal of Material Science in Semiconductor Processing* **16**:6:1538-1541

Jaehyeong L., Junsin Y.and Yan K. (2009). Effect of boron doping on the properties of chemically deposited CdS films. Chungju National University, Chungju, South Korea.

Kassim U., Narayanan H. and Anthony O. (2008). Optimization of process parameters of chemical bath deposition of Cd_{1-x} Zn_x S thin films. *Leonardo Journal of Science* **12**:111-120.

Kassim, A., Nagalingam, S., Tee, T. W., Koon, K. L., and Min, H. S (2010). *Effect of pH value and electrolyte concentration on the copper sulphide thin films prepared by chemical bath deposition method.*Gazi University, journal of science.**23** (**4**): 435-443.

Khallaf H., Chai G., Lupan O., Chow L., Heinrich H., Park L. and Schult A. (2009). Insitu boron doping of chemical-bath deposited CdS thin films. *Physics status solidi (A)* **206**:256-262

Kumar S.A., Mehra S. and Gautam T.S. (2013). Synthesis of copper sulfide (CuS) thin film by chemical bath deposition method and its characterization. *Austin Journal of Chemical Engineering* **8**:518-523

Kumar S.A., Mehra S. and Gautam T.S. (2014). Structural and optical properties of nanocrystalline Cu_xS solid thin films. *Austin Journal of Chemical Engineering* **7**:1-5

Luminita I., Ionut P. and Duta E. A. (2009). Copper sulphide (Cu_xS) thin films as possible absorber in 3D solar cells. *Energy Procedia* **2**:71-78

Makori, N.E., Oeba, D. A., & Mosiori, C. (2017). Relationship between Band gap and particle size of Cadmium sulfide Quantum Dots**.** *Chemistry Research Journal* **2**:5:15-21

Markvart T. (1998). Solar electricity. John Wiley and sons, ltd. New York. pp. 29, 33-35

Mehra S., Kumar A.S. and Thool G.S. (2014). Structural and optical properties of nanocrystalline CuxS solid thin films. *Austin Journal of Chemical Engineering* **1**:1:5

Moholkar A.V., Pawar S.M., Rajpure K.Y., Bhosele C.H. and Kim J.H. (2009). Effect of fluorine doping on highly transparent conductive spray deposited nanocrystalline tin oxide thin films. *Journal of Applied Surface Science* **255**:23:9358-9364

Morumbwa, B. R. (2013). Design and fabrication of a portable spectrophotometer to investigate optical properties of thin films. (http://irlibray.ku.ac.ke/bitsteam/handle/123 456789/6996/Murumbwa, %20%20Benard%20Riro.pdf? Sequence=1) 24, 27-28. Accessed 27th Nov, 2014

Mosiori, C. O., & Oeba, D. A. (2017). Studies on Cd1Se0. 6Te0. 4 Thin Films by Spectroscopic and Diffractometer Characterization. Traektoriâ Nauki= Path of Science, 3(9).

Mosiori, C. O., Oeba, D. A., & Shikambe, R. (2017). Determination of Planck's constant using Light Emitting Diodes. *Traektoriâ Nauki= Path of Science*, *3*(10).

Muller J., Rech B., Springer J.and Venecek M. (2004). TCO and light trapping in silicon thin film solar cells. *Journal of Solar Energy* **77**:6:917-930

Ogwu A.A., Darma T.H., and Beuquerel E. (2007).Electrical resisitivity of copper oxide thin films prepared by reactive magnetron sputtering. *Journal of Achievements in Materials and Manufacturing Engineering* **24**:172-177

Omari, M. (1975). *Elementary solid state physics*. Wisley and Sons: New York.

Osoro, O.E. (2011). Characterization of CuxOy-ZnO:Sn P-N junction for solar cell applications. (Master's Thesis). Department of Physics. Kenyatta University.

Philipps, S. (2015).Progress in Photovoltaics: Research and Applications, 1993-2015. Fraunhofer: Institute of solar cell energy.

Ramya M. and Ganesan S. (2011). Study of thickness dependent characteristics of Cu_2S thin films for various applications. *Iranian Journal of Material Science and Engineering* **8**:2:462-473

Sandeep M., (2008). Solar cells based on copper Phthalocyanine and cadmium sulphide heterojunction.Msc Thesis. University of Kentucky. Kentucky.

Saliha, I., Muhsin, Z., Yasemin, C. and Mujdat, C. (2006). *Optical characterisation of the CdZn* $(S_{1-x}Se_x)_2$ *thin films deposited by spray pyrolysis method*. Optica Applicata, **XXXVI**: 1-9.

Satosh K., Yohei S., Shotaro K., Kouichi T. and Kaoru S., (2008). Synthesis of Non-stoichiometric (LaO) CuS Thin films by Pulse Laser Deposition, *Applied Physics A: Materials Science and Processing* ***93****: 745-747.*

Sasikala, G., Thilakan, P. and Subramanian, C. (2000). Modification in the chemical bath apparatus, growth and characterization of CdS semiconducting thin films for photovoltaic applications. *Solar Energy Materials and Solar cells* **3**:62:275-293

Sumanta K.T., Rajeswari P.V. and Hota B.P. (2012). Synthesis of tin oxide film and effect of number of coating on transmittance and film thickness. *The African Review of Physics* **7**:0028:265-268

Shah, A., Torres, P., Tscharner, R., Wyrsch, N., and Keppner, H. (1999).Photovoltaic technology: the case for thin-film solar cells.Science, 285(5428), 692–698.

Takanoglu D., Yilmaz K. and Karabulut O. (2015). Structural, electrical and optical properties of thermally evaporated CdSe and in doped CdSe thin films. *Journal of Chalcogenide Letters* **12**:35-42

Tatar D., Turgut G. and Duzgun B. (2013) Effect of substrate temperature on the crystal growth orientation and some physical properties of SnO_2: F thin films deposited by spray pyrolysis technique. *Roman Journal Physics* **36**:143-153

Thanikaikarasan S., Mahilingam T., Kathalingam A., Moon H. and Yong D.K. (2010). Characterization of electrodeposited copper sulphide thin films. *Journal of New Materials for Electrochemical System* **13**:29-33

Tiwari G.N. (2009). Solar energy. Fundamentals, design, modeling and applications. *Alpha Science International* **5**:443-447

Yousaf S.A. and Ali S. (2008) .The effect of fluorine doping on optoelectronic properties of Tin dioxide (F: SnO2) thin films. (http://www.gcu.edu.pk/FullTextJour/JNSM/2008/4%20The%20Effect%20of%20Fluorine%20Doping%20on%20Optoelectronic%20Propertie.pdf) **48** no.1 and 2 pp 43-50.accessed 8th Aug.2018